1-1-2006

Design and evaluation of multi-axis vibration shaker concepts

Brinda Holur Venkatesh
University of Nevada, Las Vegas

DESIGN AND EVALUATION OF MULTI-AXIS VIBRATION SHAKER CONCEPTS

by

Brinda Holur Venkatesh

Bachelor of Engineering
University of Mysore, India
2001

A thesis submitted in partial fulfillment of the
requirements for the

Master of Science Degree in Electrical Engineering
Department of Electrical and Computer Engineering
Howard R. Hughes College of Engineering

Graduate College
University of Nevada, Las Vegas
May 2006

UNLV

Thesis Approval

The Graduate College
University of Nevada, Las Vegas

This Thesis prepared by **Brinda Holur Venkatesh**

Entitled

Design and Evaluation of Multi-Axis Vibration Shaker Concepts

was approved in partial fulfillment of the requirements for the degree of

Master of Science in Electrical Engineering

By the undersigned on April 7, 2006

Georg F. Mauer, Examination Committee Chair

Eugene McGaugh, Examination Committee Member

Sahjendra Singh, Examination Committee Member

Shahram Latifi, Examination Committee Member

Moses Karakouzian, Graduate Faculty Representative

Dean of the Graduate College

ABSTRACT

Design and Evaluation of Multi-Axis Vibration Shaker Concepts

by

Brinda Holur Venkatesh

Dr.Georg F. Mauer, Examination Committee Co-Chair
Professor
Department of Mechanical Engineering
University of Nevada, Las Vegas

and

Dr. Eugene McGaugh, Examination Committee Co-Chair
Associate Professor
Department of Electrical & Computer Engineering
University of Nevada, Las Vegas

Elastic bodies exhibit structural resonance and mode shapes at various natural frequencies. In order to avoid structural overloads and equipment malfunctions, elastic systems, mechanical and/or electrical must be evaluated and tested for their performance over the entire frequency range of their operations. Shaker systems replicate the dynamic loads encountered in a field environment, and are used for vibration testing of elastic structures. Such vibration testing ensures the reliable performance of the final product.

The objective of this research project, sponsored by the Army Research Lab (ARL), is the design and Finite Element evaluation of a new multi-axis shaker system, which will be used to test and improve the performance of mechanical and electronic components exposed to severe dynamic loading. The new shaker system should meet three major

design specifications. One, the system should have six degrees of freedom. Two, the system must work in a frequency range from 10 Hz to 3,000 Hz. Three, the system should be sturdy enough to carry payloads up to 25 lbs.

In order to develop a sound design methodology, theoretical performance predictions based on finite element analysis were compared with experimental records from an existing smaller shaker system. Structural modifications aimed at improving shaker characteristics were implemented and the performance of the modified shaker was tested experimentally. The predicted and actual dynamics of both small shaker systems were found to agree well in terms of predicting resonant modes and frequency response spectra.

ACKNOWLEDGMENTS

I would like to thank my advisor Dr. Georg Mauer for providing me with this great opportunity and guiding me to success. I am grateful to my co-advisor Dr. Eugene McGaugh, for his timely advice throughout my Master's thesis and Electrical engineering program.

I would like to express gratitude towards Mr. Bill Woyski of Team Corp. for conducting the necessary experiments on the Team Tensor and providing the results and data files whenever requested. I would like to thank Mr. Doug Lund, also from Team Corp. for helping me with the finite element modeling.

I sincerely appreciate the camaraderie of my colleagues in the Measurements lab, especially Jamil, Kofi, Vijay, Prashanth, Surya and Venkat for creating a congenial work environment. I would like to thank MSC.Software technical support team for helping me a great deal with this project, for your patience and guidance.

Very special thanks to my family and friends for everything. Lastly, I dedicate this work to my Parents, Krishna mama, Rohith & Nandu for their unconditional love and encouragement always.

TABLE OF CONTENTS

LIST OF FIGURES

LIST OF TABLES

LIST OF ACRONYMS

c:	Damping coefficient
DFT:	Discrete Fourier Transform
DSP:	Digital Signal Processing
f:	Frequency
F:	Force
FEA:	Finite Element Analysis
FEM:	Finite Element Model
FFT:	Fast Fourier Transform
g:	Acceleration of gravity, 386.087 in./sec^2
G:	Power
Hz:	Hertz
ISO:	International Standards Organization
j:	Imaginary part
k:	Spring constant
m:	Mass
MDOF:	Multiple Degrees Of Freedom
MIMO:	Multiple input, multiple output
SISO:	Single input, single output
t:	Time
x:	Linear displacement in X axis
y:	Linear displacement in Y axis
z:	Linear displacement in Z axis

LIST OF TERMINOLOGY

Acceleration: Acceleration is a vector quantity that specifies the time rate of change of velocity.

Accelerometer: An accelerometer is a transducer whose output is proportional to the acceleration input.

Amplitude: Amplitude is the maximum value of a sinusoidal quantity.

Angular Frequency: The angular frequency of a periodic quantity, in radians per unit time, is the frequency multiplied by 2π .

Autocorrelation Function: The autocorrelation function of a signal is the average of the product of the value of the signal at time t with the value at time $t+\tau$: $R(\tau) = \overline{x(t)x(t+\tau)}$

For a stationary random signal of infinite duration, the power spectral density (except for a constant factor) is the cosine Fourier transform of the autocorrelation function.

Autospectral Density (*power spectral density)*: The limiting mean-square value (e.g. of acceleration, velocity, displacement, stress, or other random variable) per unit bandwidth, i.e. the limit of the mean-square value in a given rectangular bandwidth divided by the bandwidth, as the bandwidth approaches zero.

Auxiliary Mass Damper (Damped Vibration Absorber): An auxiliary mass damper is a system consisting of a mass, spring, and damper which tend to reduce vibration by the dissipation of energy in the damper as a result of relative motion between the mass and the structure to which the damper is attached.

Center-of-Gravity: CG is the point through which passes the resultant of the weights of its component particles for all orientations of the body with respect to a gravitational field; if the gravitational field is uniform, the CG corresponds with the Center-of-Mass.

Correlation Function: The correlation function of two variables is the average value of their product ($\overline{x_1(t)x_2(t)}$).

Coupled Modes: Coupled modes are modes of vibration that are not independent but which influence one another because of energy transfer from one mode to the other.

Critical Damping: Critical damping is the minimum viscous damping that will allow a displaced system to return to its initial position without oscillation.

Damper: A damper is a device used to reduce the magnitude of a shock or vibration by one or more energy dissipation methods.

Degrees-of Freedom: The number of degrees-of-freedom of a mechanical system is equal to the minimum number of independent coordinates required to define completely the positions of all parts of the system at any instant of time. In general, it is equal to the number of independent displacements that are possible.

Deterministic Function: A deterministic function is one whose value at any time can be predicted from its value at any other time.

Displacement: Displacement is a vector quantity that specifies the change of position of a body or particle and is usually measured from the mean position or position at rest.

Distortion: Distortion is an undesirable change in waveform. Noise and certain desired changes in waveform, such as those resulting from modulation or detection, are not usually classed as distortion.

Dynamic Vibration Absorber (Tuned Damper): A dynamic vibration absorber is an auxiliary mass-spring system which tends to neutralize vibration of a structure to which it is attached. The basic principle of operation is vibration out-of-phase with the vibration of such structure, thereby applying a counteracting force.

Effective Bandwidth: The effective bandwidth of a specified transmission system is the bandwidth of an ideal system which (1) has a uniform transmission in its pass band equal to the maximum transmission of the specified system and (2) transmits the same power as the specified system when the two systems are receiving equal input signals having a uniform distribution of energy at all frequencies.

Effective Mass: The complex ratio of force to acceleration during simple harmonic motion.

Equivalent System: An equivalent system is one that may be substituted for another system for the purpose of analysis.

Excitation: Excitation is an external force (or other input) applied to a system that causes the system to respond in some way.

Filter: A filter is a device for separating waves on the basis of their frequency. It introduces relatively small gain to waves in one or more frequency bands and relatively large gain to waves of other frequencies.

Forced Vibration: The oscillation of a system is forced if the response is imposed by the excitation. If the excitation is periodic and continuing, the oscillation is steady-state.

Foundation: A foundation is a structure that supports the gravity load of a mechanical system. It may be fixed in space, or it may undergo a motion that provides excitation for the supported system.

Frequency: The frequency of a function periodic in time is the reciprocal of the period. The unit is the cycle per unit time and must be specified; the unit *cycle per second* is called *hertz* (Hz).

Induced Environments: Induced environments are those conditions generated as a result of the operation of a structure or equipment.

Isolation: Isolation is a reduction in the capacity of a system to respond to an excitation, attained by the use of a resilient support.

Linear System: A system is linear if for every element in the system the response is proportional to the excitation. This definition implies that the dynamic properties of each element in the system can be represented by a set of linear differential equations with constant coefficients, and that for the system as a whole superposition holds.

Mechanical System: A mechanical System is an aggregate of matter comprising a defined configuration of mass, stiffness, and damping.

Mode of Vibration: In a system undergoing vibration, a mode of vibration is a characteristic pattern assumed by the system in which the motion of every particle is simple harmonic with the same frequency. Two or more modes may exist concurrently in a multiple degree-of-freedom system.

Multiple Degrees-of-Freedom System: A multiple degree-of-freedom system is one for which two or more coordinates are required to define completely the position of the system at any instant.

Natural Frequency: Natural frequency is the frequency of free vibration of a system. For a multiple degree-of-freedom system, the natural frequencies are the frequencies of the normal modes of vibration.

Oscillation: Oscillation is the variation, usually with time, of the magnitude of a quantity with respect to a specified reference when the magnitude is alternately greater and smaller than the reference.

Random Vibration: Random vibration is vibration whose instantaneous magnitude is not specified for any given instant of time. The instantaneous magnitude of a random vibration is specified only by probability distribution function giving the probable fraction of the total time the magnitude lies within a specified range.

Resonance: Resonance of a system in forced vibration exists when any change, however small, in the frequency of excitation causes a decrease in the response of the system.

Stiffness: Stiffness is the ratio of change of force (or torque) to the corresponding change on translational (or rotational) deflection of an elastic element.

Time History: The magnitude of a quantity expressed as a function of time.

Transducer: A transducer is a device which converts shock or vibratory motions into an optical, a mechanical, or most commonly to an electrical signal that is proportional to a parameter of the experienced motion.

Transfer Impedance: Transfer impedance between two points is the impedance involving the ratio of force to velocity when force is measured at one point and velocity at the other point. The term transfer impedance is also used to denote the ratio of force to velocity measured at the same point but in different directions.

Transmissibility: Transmissibility is the nondimensional ratio of the response amplitude of a system in steady-state forced vibration to the excitation amplitude.

Uncorrelated: Two signals or variables $x_1(t)$ and $x_2(t)$ are said to be uncorrelated if the average value of their product is zero. If the correlation coefficient is unity, then the signals are said to be completely correlated.

Vibration: Vibration is an oscillation wherein the quantity is a parameter that defines the motion of a mechanical system.

Vibration Machine: A vibration machine is a device for subjecting a mechanical system to a controlled and reproducible mechanical vibration.

Viscous Damping: Viscous damping is the dissipation of energy that occurs when a particle in a vibrating system is resisted by a force that has a magnitude proportional to the magnitude of the velocity of the particle and direction opposite to the direction of the particle.

CHAPTER 1

INTRODUCTION

Shaker Systems are used for the vibration testing of structures. Vibration testing is the shaking or shocking of a component or an assembly to see how it will stand up to the real world conditions [1, 2, 3]. It is an important step in the design and development of any new product that could fail when exposed to vibrations [1, 2].

Some tests are as simple as dropping the product from a certain height, or loading it into a truck and driving it on rough roads. Others are more complicated like duplication of the vibration history of an airplane or the stress experienced by vehicle tires.

Vibration testing is required for military equipment, in the aerospace industry, the automotive industry, and for commercial and consumer electronics. The process of vibration testing is depicted in Figure 1.1.

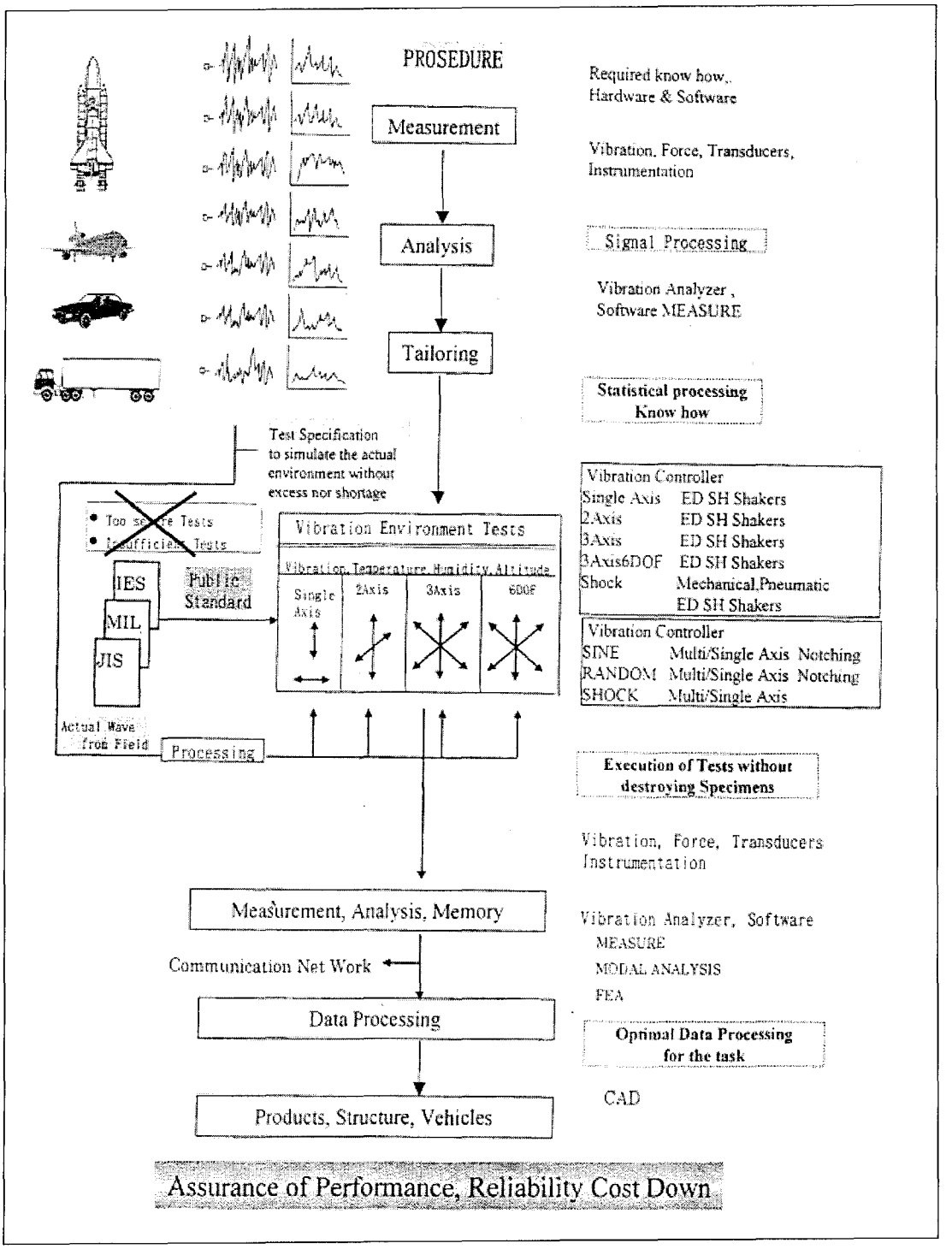

Figure 1-1: Vibration Testing Process, [4]

1.1 Vibration Testing Procedures

A typical vibration testing system consists of three groups of hardware:

- An excitation group comprised of a signal generator, a power amplifier and one or more actuators, e.g. electrodynamic shakers,
- A feedback circuit made up of one or more accelerometers, signal conditioning and monitoring units, and
- A controller. The controller can be analog or digital. Different control algorithms exist for sinusoidal and random vibration testing.

The shaker systems are designed to produce vibrations consistent with mathematical models or recorded time histories from experiments. *MIL std.802.11* depicts a possible vibration-testing scenario which is shown in Figure 1-2. First the real world vibration data are acquired using a portable recording device. The shaker test should expose the test article to the power density spectrum found under operating conditions. The controller computes the drive signals applied to the shaker system. The controller measures the output. The controller iteratively modifies the drive signal such that the tested system's output power density spectrum agrees as closely as possible with specifications.

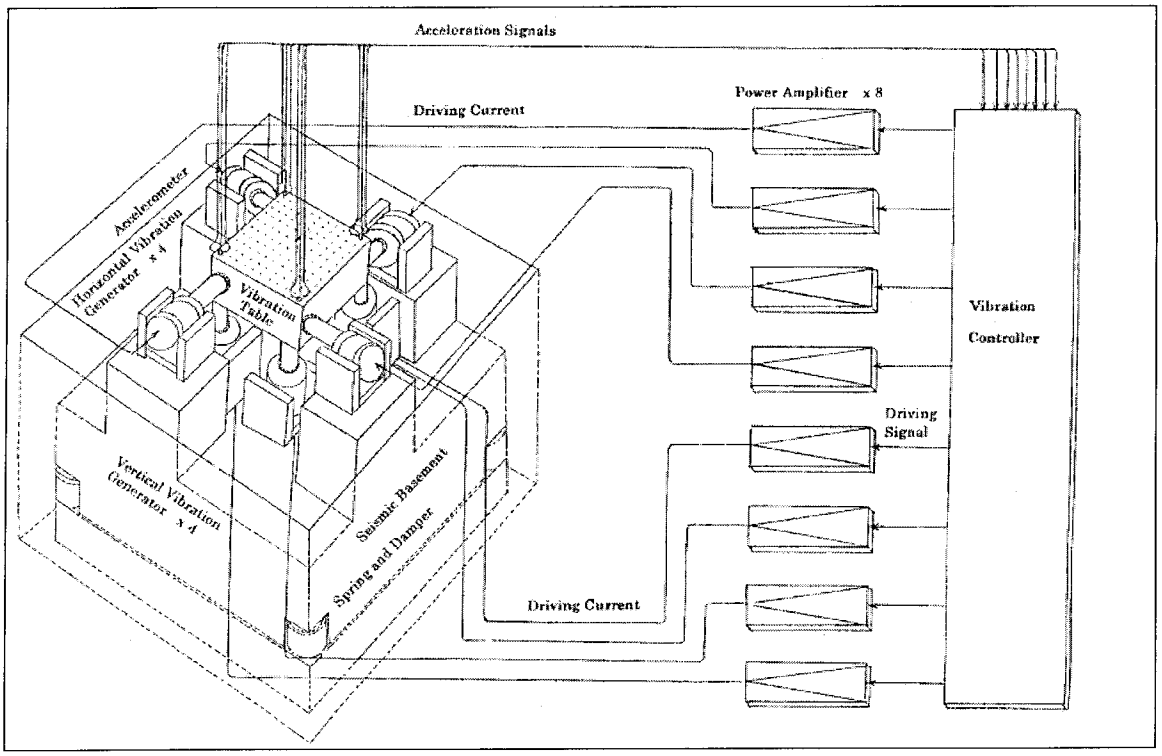

Figure 1-2: Hydraulic Six- Axis Shaker, [5]

Historically, products were tested first using single-axis actuation. It has been proven that multi-axis testing provides a more realistic representation of actual field conditions [4]. In many cases, field failures can be repeated only when vibration is applied in all coordinate directions simultaneously. For example, triaxial excitation can cause twice the fatigue damage as similar test amplitudes and duration in single axis testing [ISO Standard 2631-1]. Thus multi-axis testing is replacing uniaxial systems in many applications.

Random vibration testing is more predominant these days simply because it excites all test specimen resonance in the applied spectrum simultaneously, which is much more realistic when compared to sine testing [1, 2, 3, 5, 6].

Usually most shakers have equal number of transducers and exciters. This is termed as "Square" arrangement. It has been proved that "Rectangular" arrangement where there are more controllers than exciters, is a better technique to control multi-input multi-output shaker systems [7].

This type of control will be useful and practical for MIMO testing where 2 electrodynamic shakers will be used in a single, usually vertical, axis such as missile transportation or airborne applications. Traditional control in these cases, were to place two accelerometers near the two attachment points or exciters. Several Limit Channels were defined along with these two Control Channels. But limit control is known to reduce the excitation levels and create uneven motion on the test article, whereas Adaptive Rectangular Control has proven to a more uniform motion on the shaker table and the test article. TEAM TENSOR, the shaker under analysis has 16 accelerometers and 6 exciters.

Due to the mismatch between the number of exciters and number of sensors, controlling these multi degree of freedom (MDOF) shakers becomes a difficult task. A method to transform the response from multiple control transducers and the actuation capability of the multiple actuators that are being used from actuator space to MDOF space and vice versa to effectively perform these MDOF tests has been developed [8].

1.2 Motivation

The DOD objective of increasing the reliability of smart ammunitions and critical vehicle components requires the realistic testing of prototypes under duplicate field vibrations. The DOD wishes to conduct multi-axial tests at frequencies up to 2 kHz.

The existing multi-axis devices are either costly and/ or do not satisfy the MIL-STD specifications for vibration testing. The development of shaker concepts capable of meeting the rigorous military specifications requires an in-depth evaluation of controls, excitation, and spatial-motion drive technologies.

The work described in this thesis has been funded by the US Army Research Lab with the objective of analyzing an existing shaker developed by the TEAM Corp. of Burlington, WA, with the eventual goal to develop a 6-axis shaker system for payloads to 25-lbs. The existing 5-lbs payload Team shaker system operates at frequencies ranging from 10 Hz to 3000 Hz [9].

1.2 Problem Definition

The wider project objective is the design and analysis of shaker design configurations for the vibration testing of mechanical and electronic components. As a minimum the shaker should meet the following specifications:

- Shaker generating 6 Degree-of-Freedom (DOF) vibration with complete, simultaneous control of the amplitudes and phase angles of all 6 degrees of freedom.
- Accelerations in six directions simultaneously to 50 g
- Frequency range 10 Hz-3000 Hz
- Payload up to 25 lbs
- The current uniaxial testing method does not adequately reproduce the multi-axis vibration environments that prevail in operating conditions.
- Multi-axial vibrations dominate the typical operating environments.

- Existing multi-axis devices are either costly and/or inadequate in meeting MIL-STD vibration test requirements.
- Reduce test time by 67% compared to uniaxial testing

In general, it is difficult to predict resonant frequencies above 500 Hz in shaker systems. Thus it is hard to design a shaker system which will satisfy the above requirements. In order to save time and money, the capabilities of **F**inite **E**lement **A**nalysis (FEA) are explored in this project.

Our project seeks to model and analyze an existing electrodynamic six-axis shaker system, developed by TEAM Corp. The TEAM shaker system is excited at 6 spatial locations by electrodynamic actuators. The analytic model is to be compared to experimental results recorded on the TEAM shaker system. These experiments were conducted by Mr. Bill Woyski and Mr. Doug Lund of Team Corp.

The analytic model should be sufficiently detailed and accurate so as to predict the experimental response within narrow error bands. The validated analytic model would then serve as a basis for designing larger multi-axis shaker systems.

1.3 Thesis Outline

This thesis is divided into six Chapters. The first chapter presents an introduction to vibration testing and defines the project objectives. The second chapter describes the important features of hydraulic and electrodynamic shaker systems. Chapter three describes the physical setup and the Finite Element (FE) modeling of the shaker system. The fourth chapter explains the sensor placement, input signals, controller, experimental setup and various mathematical analysis procedures relevant to this work. The fifth

chapter discusses the experiments conducted at TEAM, corresponding simulations at UNLV and the results obtained. The power density spectra of experimental records are compared with the simulation results. Conclusions and proposed future work are presented in the sixth chapter.

CHAPTER 2

SHAKER SYSTEM

This chapter presents a brief discussion of the principles of hydraulic and electric shaker systems, followed by a detailed study of electrodynamic shakers. *Harris* (2002) provides a good understanding of the vibration current shaker technology.

2.1 Hydraulic Shaker

Hydraulic shakers generate large forces and amplitudes as required in testing large aerospace or marine structures, automotive industry, and seismic testing or in applications where the magnetic fields of the electrodynamic shakers cannot be tolerated [2, 3, 5]. The hydraulic actuators are small in relation to the force attainable. A firm ground or a large massive base is necessary to anchor the shaker. The useful frequency range is generally limited to about 500 Hz.

Figure 2-1 depicts a 40-ton hydraulic shaker installed in China for seismic testing. Eight servo hydraulic actuators drive the table with 4 vertical actuators and 2 pairs of horizontal actuators. Frequencies range from 0.1 Hz to 100 Hz with maximum displacement of greater than 200 mm p-p. Loads up to 60 tons can be accommodated [5].

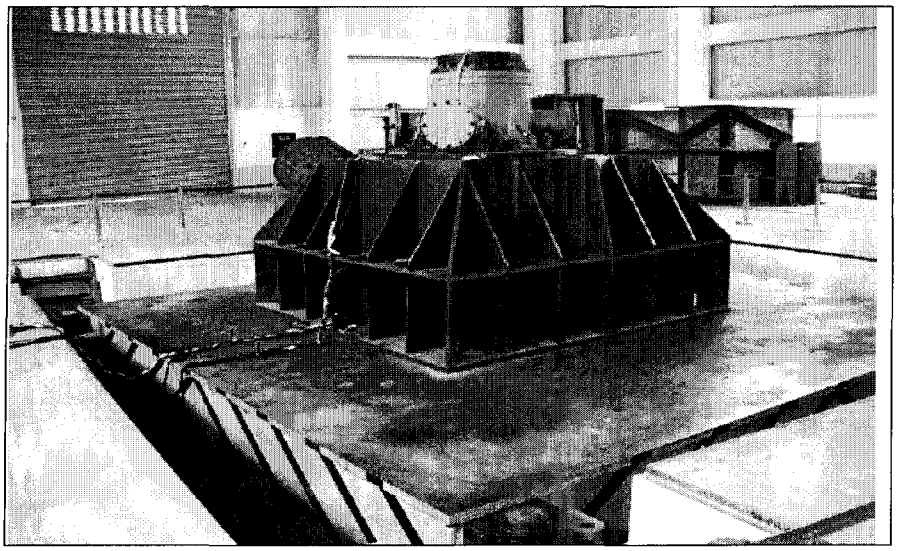

Figure 2-1: Hydraulic Shaker for Seismic Testing

The *CUBE*, manufactured by TEAM Corporation, is a 6 DOF hydraulic device, which permits testing up to 250 Hz in sine, expandable to 500 Hz when using random testing in the vertical axis. The 6 servo hydraulic actuators are situated inside the shaker structure [9].

2.2 Electrodynamic Shaker

Electrodynamic multi-shaker systems have the advantages of high frequency capabilities and linearity in a wide dynamic range.

Jens T. Broch and *George Fox Lang* explain in detail the important design factors of these devices. The structure of an electrodynamic shaker is similar to a loudspeaker [3, 10, 11, 12]. It has a coil of wire suspended in a fixed radial magnetic field. When a current is passed through this coil, an axial force F, is produced proportional to the current I, the magnetic flux B, passing through the coil and the length L of the wire within the flux field. Laplace law states that the force on the current wire is: $F = B\,I\,L$. The coil,

coil form and the table structure comprise the armature assembly on which the test object is mounted.

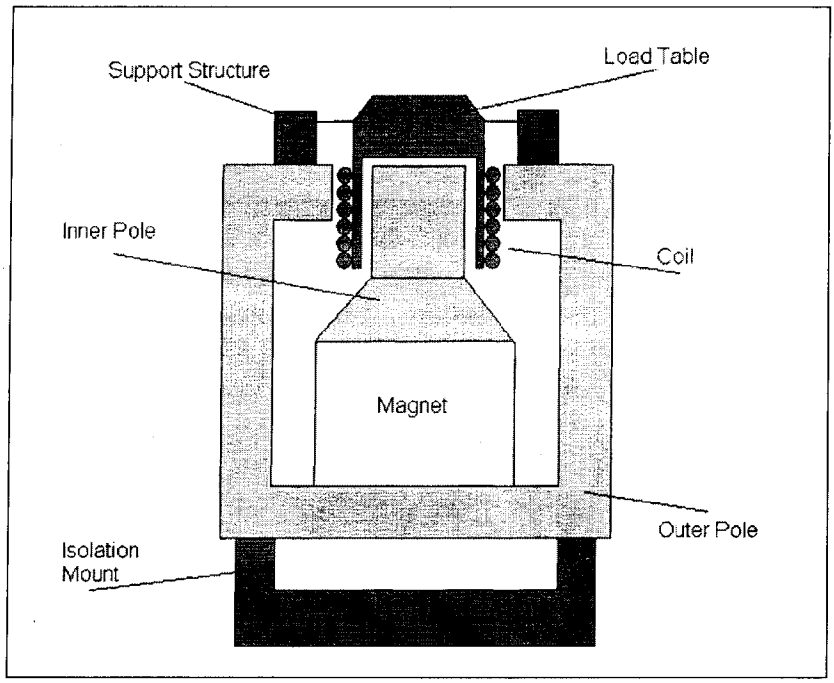

Figure 2-2: Electrodynamic Shaker [10]

The performance envelope of an electrodynamic shaker system is strongly influenced by three modes of vibration namely Isolation mode, Suspension mode (low frequency modes) and Coil mode which occur at higher frequencies [3, 10, 11, 12].

Other limiting factors are the voltage/current capacities of the power amplifier that drives it, designed stroke (displacement) of the table, the moving mass and total mass of the shaker, the thermal power limit of the coil and the stress safety factor of the armature [10, 11, 12, 13].

An electrodynamic shaker is usually modeled as electromechanical system with experimentally derived two-port network. This depends on the characteristics of both, the shaker and the load. This characterization in turn depends heavily on the accurate

measurement of the input voltage and current along with the accelerations of the shaker armature. Thus measuring both current and voltage is advisable [14].

2.4 TEAM TENSOR

Team Corporation's TENSOR is a 6-DOF electrodynamic shaker system. The TENSOR's load table (termed 'center member' in the following chapters) and actuators are assembled in a tight, compact package. The compact design results in considerable table stiffness and comparatively high-frequency modes [9].

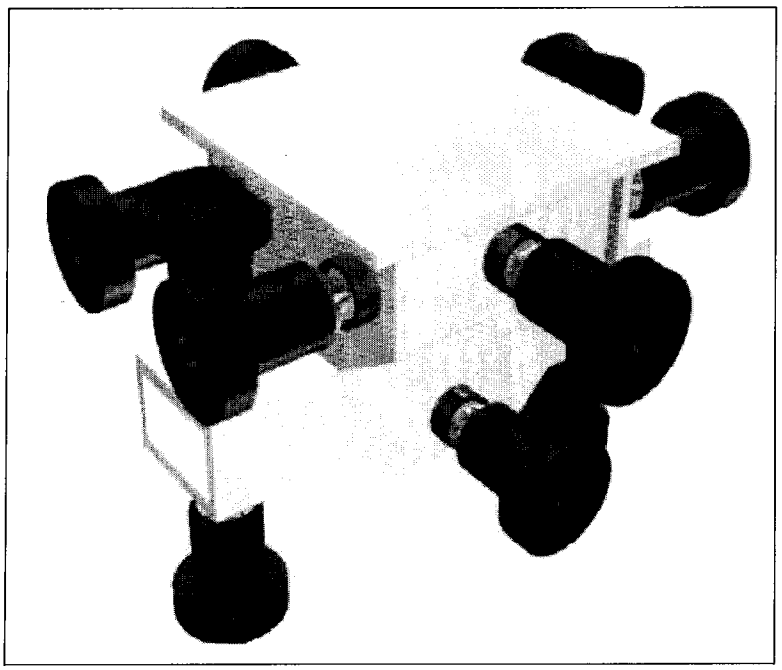

Figure 2-3: Team TENSOR Multi-Axis Test System

Referring to Fig. 2.3, each actuator operates in compression mode, with pre-loaded springs at opposing sides. In equilibrium, each pair of springs applies a constant pre-load. The drive signal generates forces which move the table from the equilibrium position.

Two equal actuator signals in the same coordinate direction cause pure translational motion when applied in phase. Phase differences between two equal actuator signals in the same coordinate direction cause rotation as well as translation.

CHAPTER 3

ANALYTIC MODEL OF THE SIX-AXIS SHAKER SYSTEM: FINITE ELEMENT ANALYSIS

This chapter discusses the mechanical structure of the shaker table and its finite element model in detail. The main part of interest of the electrodynamic shaker system is the center member. The original structure is as shown below.

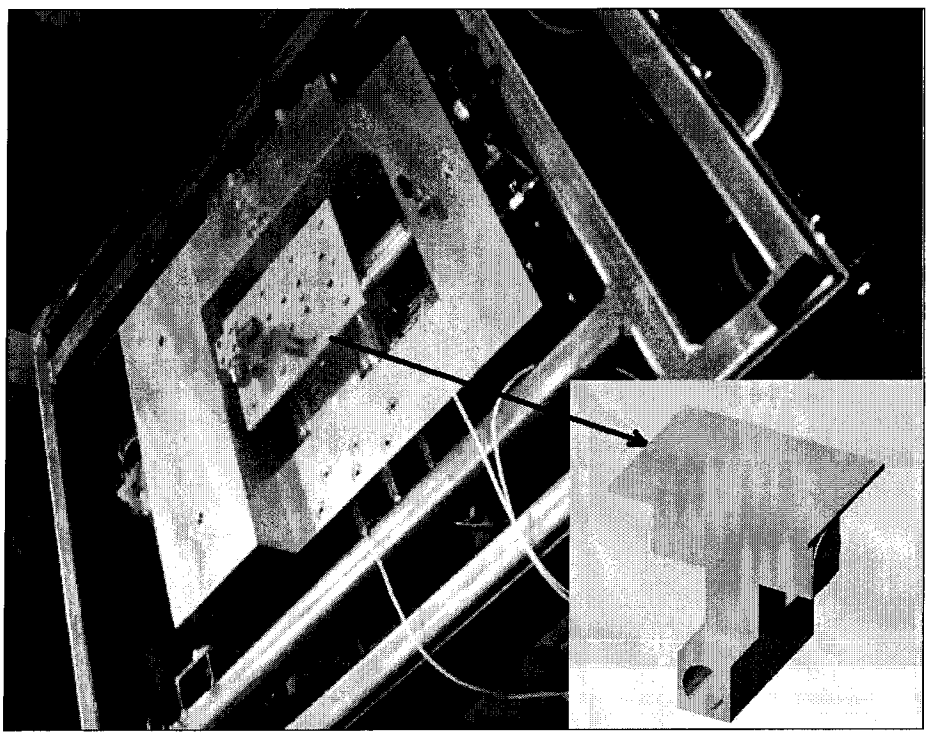

Figure 3-1: TEAM TENSOR

FEA is a mathematical technique for analyzing stress, which breaks down a physical structure into substructures called "finite elements." The finite elements and their interrelationships expressed as a matrix equation and solved mathematically. The material properties and boundary conditions are considered over these elements and expressed in terms of unknown values at element corners. This results in a set of equations, the solution to which gives us the approximate behavior of the system [15]. In essence a computer model of a material or design is stressed and analyzed for specific results [2, 15].

We used the graphical user interface MSC.Patran for preprocessing and post processing work. The solver was MSC.Nastran with MSC.Marc preference. The whole finite element analysis process is divided into several smaller tasks, which are explained below:

- The geometry, shown in Figure 3.2 was created in Solidworks.
- Imported into Patran.
- System modeling.
- Meshing the model
- Define physical elemental properties
- Apply load and boundary conditions
- Finite Element Analysis

3.1 Geometry

The center member is made up of magnesium AZ31B. This material was chosen because of its low density and high strength. The physical dimensions of the center

member are shown below in Figure 3-2. All the dimensions are in US Customary units. The table is 8 inches in height. The tabletop measures 6.5 by 8.5 inches. There are 6 electrodynamic actuators. Two in each X, Y, and Z direction. There are two preloaded springs opposing each of these actuators. They are made of spring-steel. One end of each of these springs is fixed to the ground. These springs and actuators are in contact with the table through a viscous oil film.

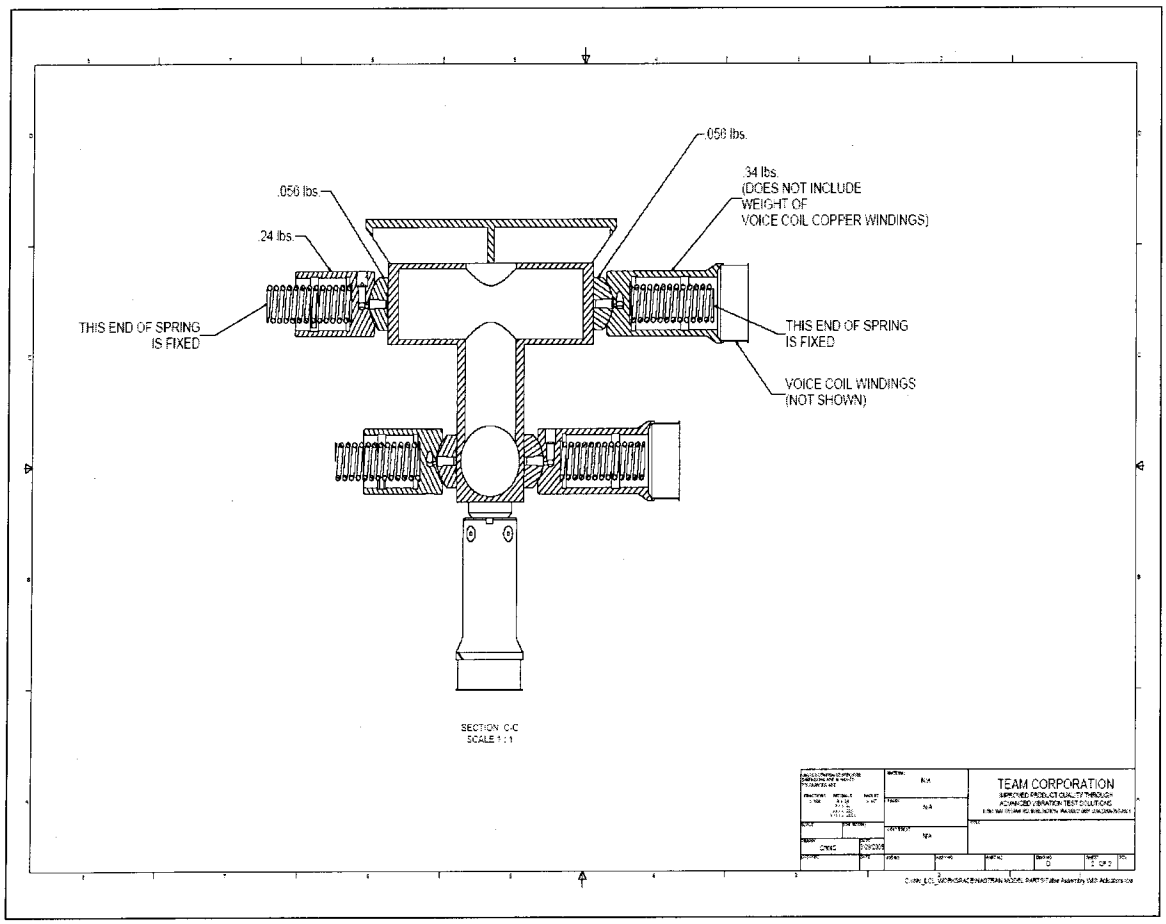

Figure 3-2: Engineering Drawing of the Center Member [9]

The design and setup of the real system has been explained above in the engineering drawing. This system was modeled in Patran in preparation for the FE analysis. As seen in Fig. 3-2, the moving parts consist of one single solid body (center member) surrounded by actuators, springs, dampers, pre-loads and constraints. The following sections discuss the meshing of the solid body, assignment of the material and element properties, and then the modeling of the whole system along with the pre-loads and boundary conditions.

3.2 Meshing the Model

Meshing is a process of breaking up a physical domain into several small sub-domains in order to facilitate the numerical solution of a partial differential equation. Most meshing algorithms use the "bottoms up" method. Nodes are placed at all vertices, and then they are distributed along the curves. The result of the curve meshing process provides input to a surface-meshing algorithm, which decomposes the surface into triangular and quadrilateral elements. Finally, if the body is a solid entity then a set of meshed areas defining a closed volume is fed to the volume mesher for the generation of different solid element types. Either we can specify the kind of elements, number of elements in various parts of the body or we can use automatic meshing options available in all commercial softwares.

The meshed center member is shown in Figure 3-4 below. We first divided the whole body into several smaller and simpler geometric shapes in order to obtain a nice and even mesh. The body is divided into tetrahedral elements. Each element connects 10 nodes. The meshed center member has 16000 elements and 30000 DOFs.

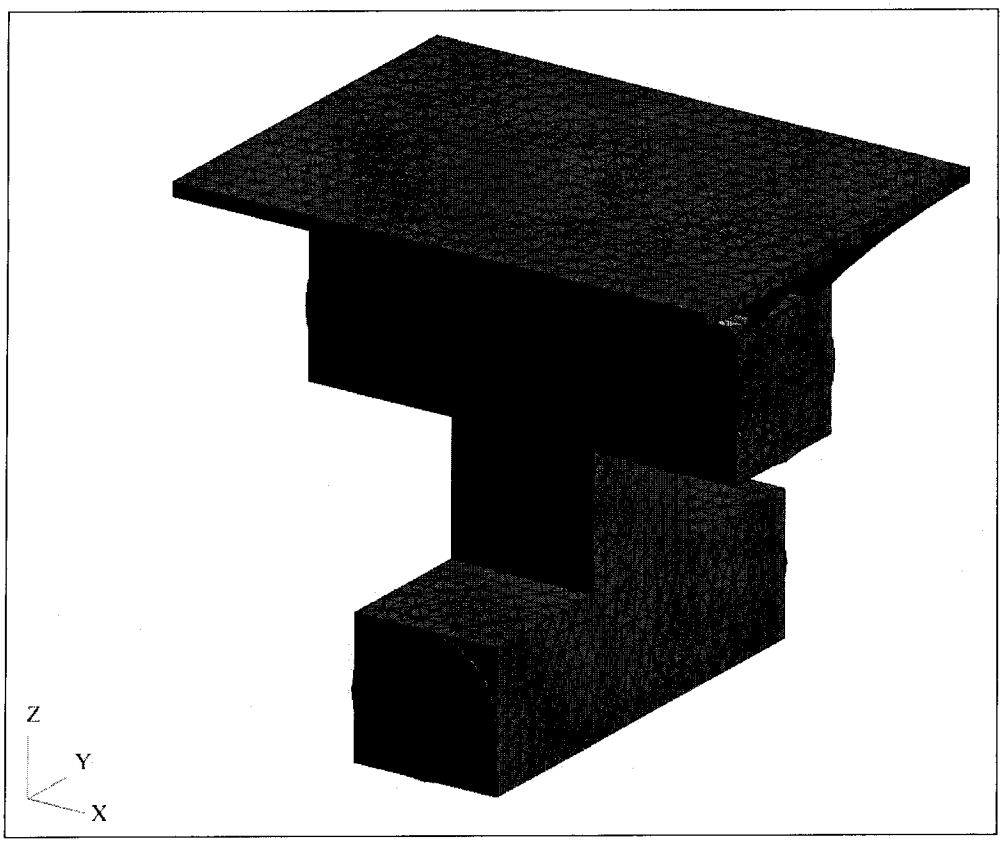

Figure 3-3: Meshed Model

3.3 Physical Properties

Constitutive Model:	Linear Elastic
Property Name	Value
Elastic Modulus =	6500000.
Poisson Ratio =	0.34999999
Shear Modulus =	
Density =	0.000165541
Thermal Expan. Coeff =	1.41E-005
Structural Damping Coeff =	0.001
Reference Temperature =	70.

Figure 3-4: Magnesium Az31B Properties as entered in Patran Database

3.4 System Modeling

Two finite element models for this analysis were considered. The first one is the exact replication of the Tensor system while the second is a simplified version. The geometry of the center member and meshing are identical in both models. The major difference between the two FE models lies in the definition of the contacts between the sliding surfaces. This is explained below in subsections 3.4.1 and 3.4.2.

3.4.1 Nonlinear Model

12 small rigid mass-less surfaces are added to the FE model, see Fig. 3.5. The contact between the deformable center member and these rigid surfaces is defined as a sliding contact with a friction coefficient of zero. This contact definition makes the FE model non-linear and thus complex to analyze. We used the nonlinear solver MSC.Marc, along with MSC.Nastran for the simulations.

The springs are modeled by beam elements, made up of spring-steel material. These springs are attached to the center of the rigid surfaces. The other ends of these beam elements are attached to another smaller beam element. One end of these smaller beam elements is completely fixed to the ground while the other end has 4 degrees of freedom: three rotational and one translational. The spring and the rigid plate are constrained in their respective X-Y plane.

The nonlinear system has boundary nonlinearity, which is due to the contact between the actuators and the table. When in contact, mechanical loads and perhaps heat are transmitted across the area of contact. If friction is present, shear forces are also transferred. Both deformable-to-rigid and deformable-to-deformable contact situations can be modeled in MARC.

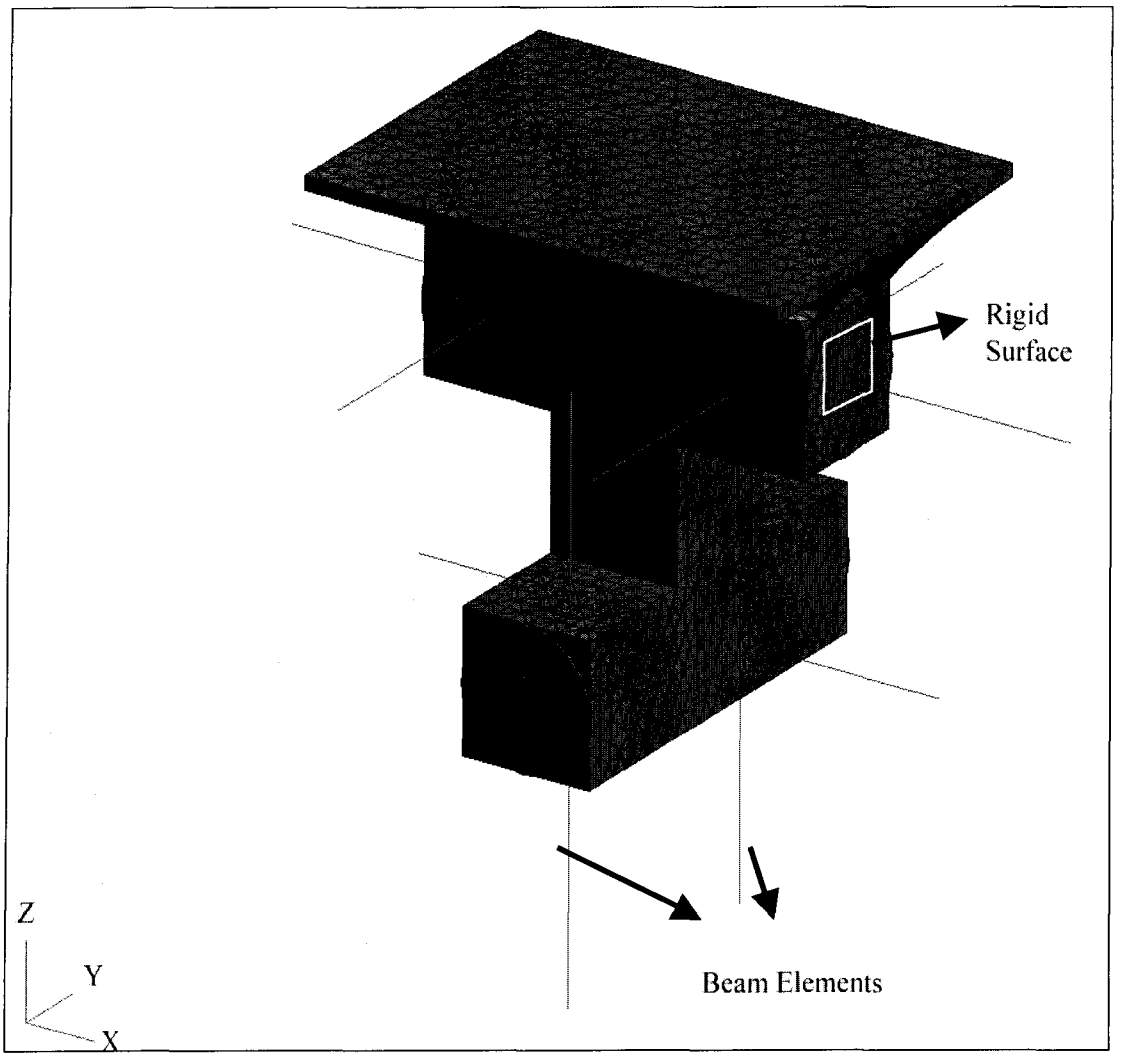

Figure 3-5: Model with Rigid Surfaces and Beam Elements

3.4.2 Linearized Model

Doug Lund from TEAM has developed the simplified structure. Here a cluster of rigid elements is attached to the surface of the center member at each of the 12 pad bearing locations. These rigid elements have no mass. Instead of beam elements, the inbuilt linear spring elements are used. Each end of the spring element acts like a ball joint, transmitting only axial forces.

A single mass element represents the total moving mass of the actuator. A second mass element represents the mass of the preload piston. These single mass elements are constrained to allow uniaxial motion only in the direction parallel to the linear spring element. The linear model simulates the sliding surface contact without using nonlinear elements.

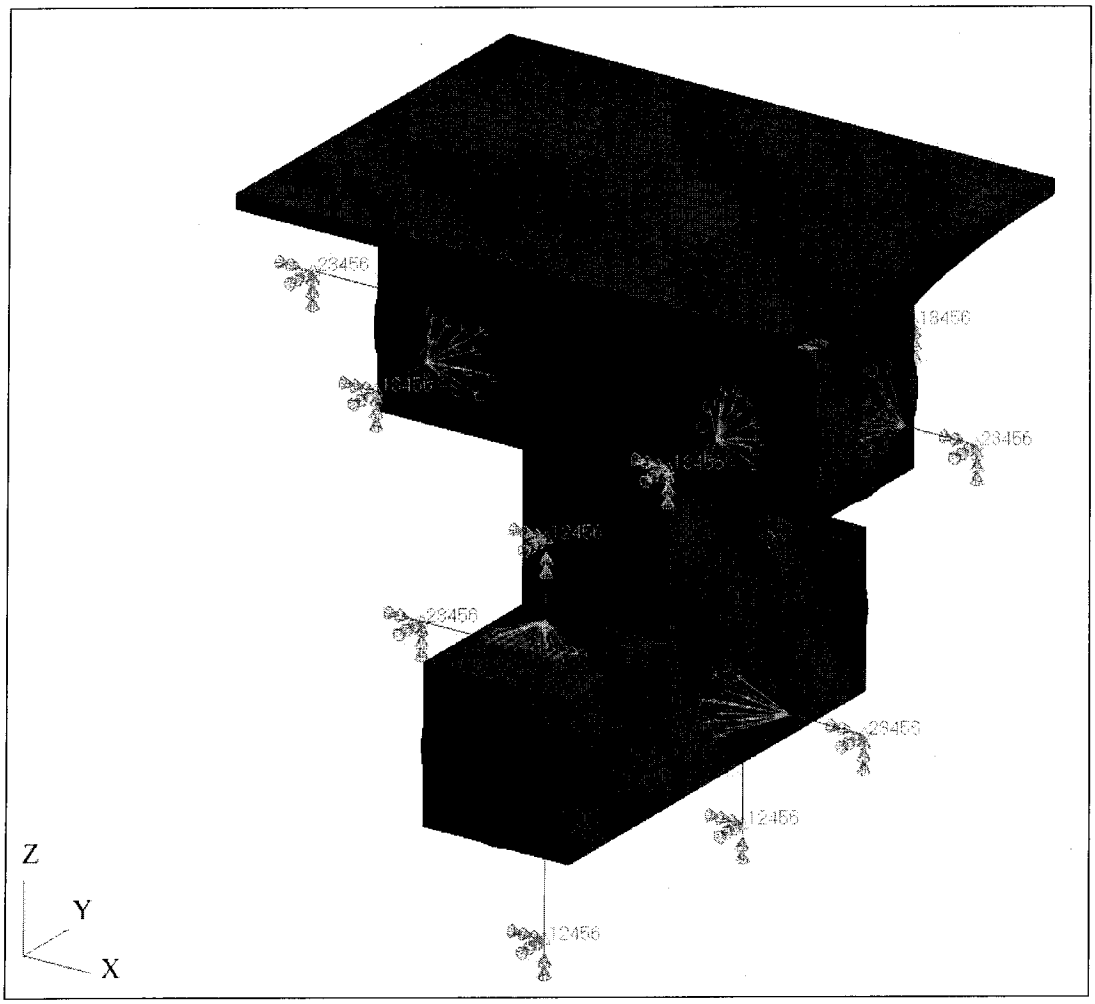

Figure 3-6: Model with Rigid Elements and Linear Springs

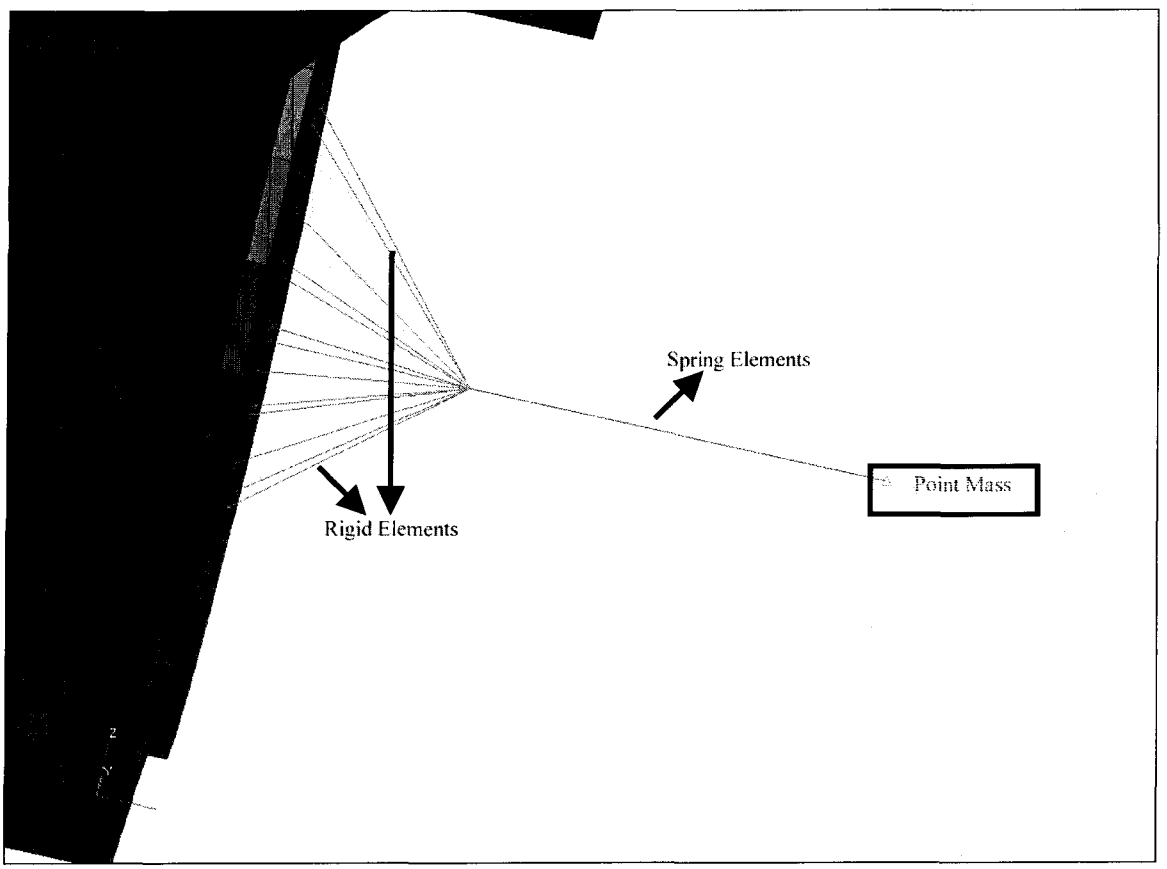

Figure 3-7: Inset from Figure 3.6

3.5 Load & Boundary Conditions:

A preload of 90 lbs is applied at the end of each spring element in the nonlinear model. The preloads are not considered in the linear model since the equal and opposite preloads cancel each other.

The sinusoidal excitation force is applied at the center of the surface where the beam is connected. In the linear system, the sinusoidal force is applied where the spring element is connected to the cluster of rigid elements.

3.6 Comparing the Two Models using Transient Analysis

Transient Analyses were conducted on both systems. The input was a single frequency sine wave of 1000 Hz. The simulation was conducted for 0.05 seconds. Nastran took 48 hours for the complex model and 6 hours for the simplified one. The linear analysis proved to be approximately 8 times faster than the nonlinear analysis. The output acceleration at point 8 (corner pt on table top) is shown below. The results from both FE models are nearly identical, and indistinguishable from another in Fig. 3.7, confirming that the simplified model does portray the contacts correctly.

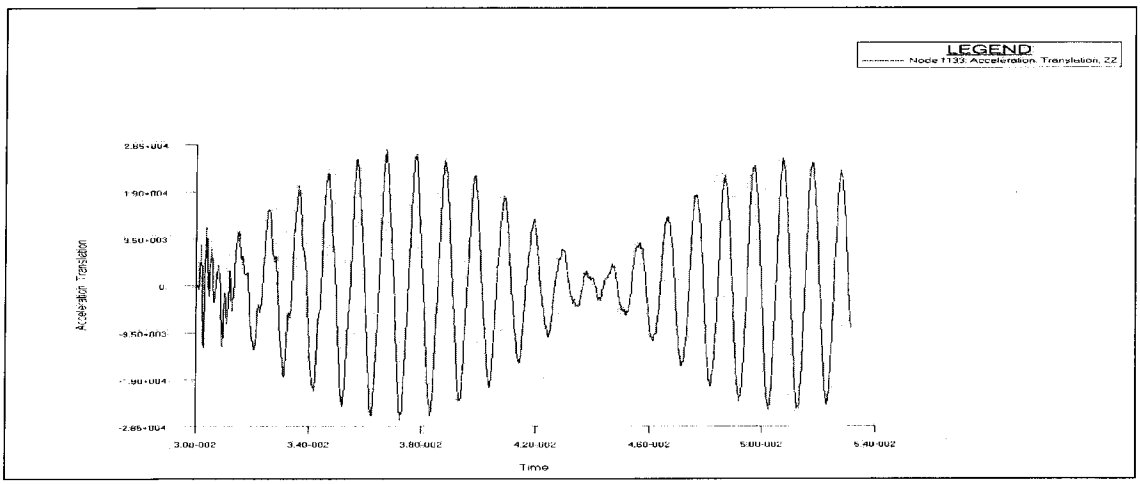

Figure 3-8: Time Response from both FE Models

Figure 3-7 shows a transition period of 0.03 seconds before the output reaches a steady state response. We also observe a second frequency along with the expected 1000 Hz signal. The 50-Hz envelope seen in Fig. 3-7 results from the undamped resonant spring elements attached to the body. The 50Hz resonance was not observed experimentally. The addition of viscous damping in parallel to the springs, as shown Figure 3-8, eliminated the resonance. The transitory oscillations disappear completely

after 0.08 seconds. Fig. 3.9 shows the time-domain response to a 1,000 Hz drive signal after viscous damping was added.

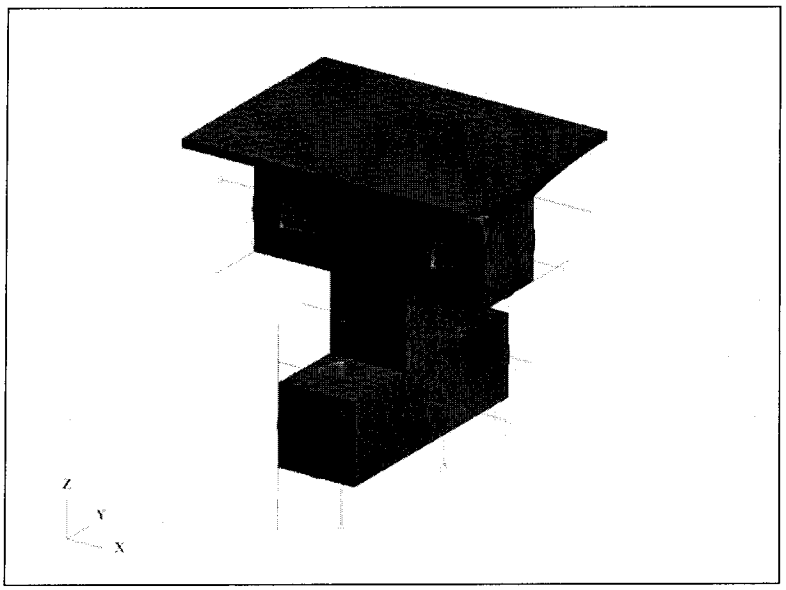

Figure 3-9: Dampers Added to the Simplified Model

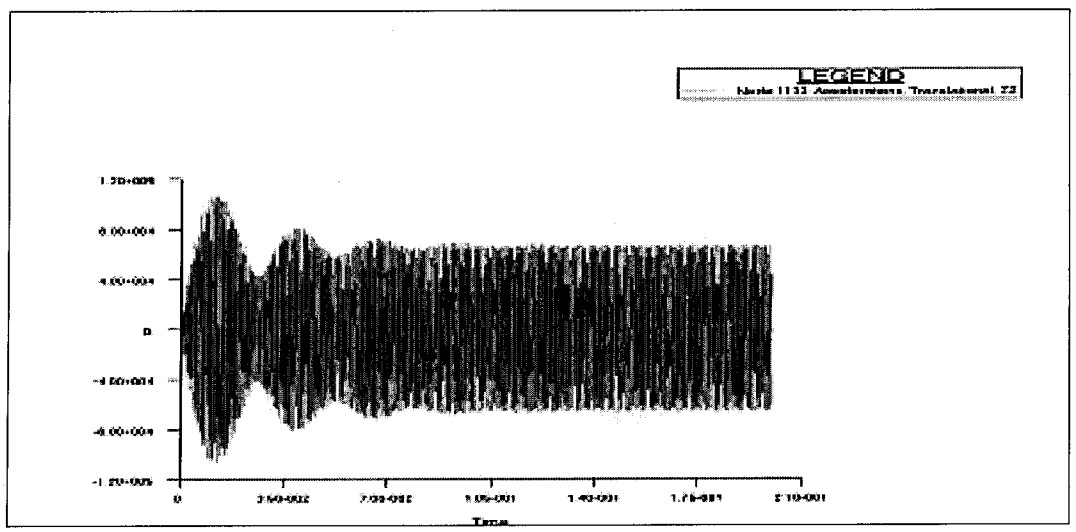

Figure 3-10: Time Response after Adding Dampers

CHAPTER 4

SPECTRAL ANALYSIS

4.1 Quantitative Descriptions

The complete definition of a vibration condition requires the description of magnitude and its variation with both frequency and time. Vibration data can consist of deterministic, random and mixed signals. The following sections provide an overview of the statistical operations performed on such data [2, 16, 17, 18]. These theories and equations were extensively used to obtain the results presented.

4.1.1 Fourier Transform

The Figure 4-1 shows the transformation of a vector *x(t)* from time domain to frequency domain and vice versa. Discrete Fourier Transforms (DFTs) are applied to the signals recorded over a time period *T*. Standard DSP uses *lower case letters* to represent time domain information such as $x(n\Delta t)$, and *upper case letters* to represent frequency domain information that is $X(n\Delta f)$ [18].

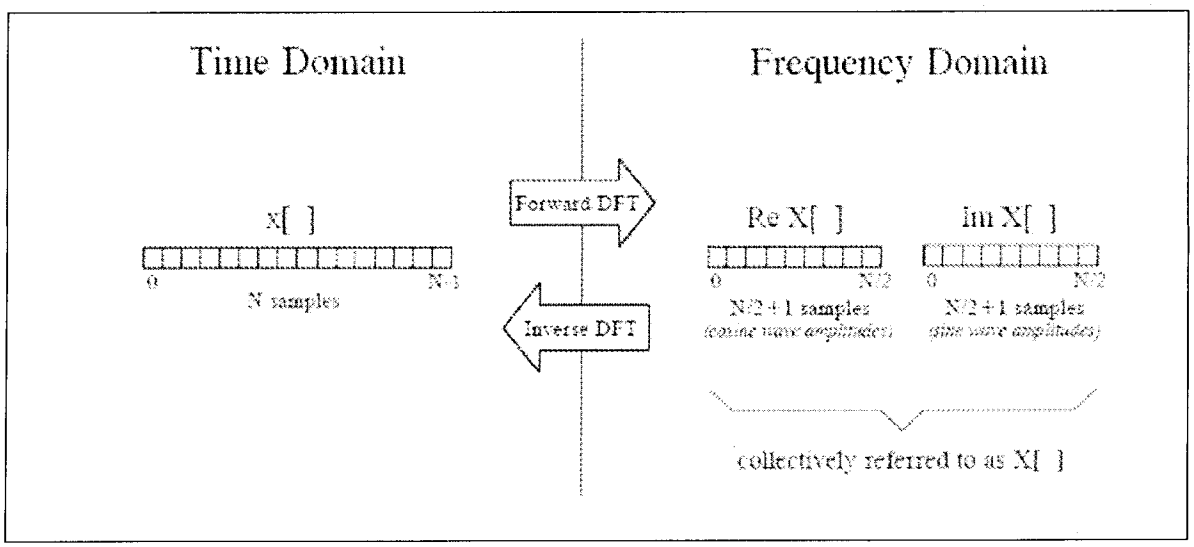

Figure 4-1: Discrete Fourier Transforms [18]

The following relationships [2, 16, 17, 18] apply:

$$X(m\Delta f) = \Delta t \sum_{i=0}^{N-1} x(n\Delta t) e^{-i2\Pi m\Delta f n\Delta t} \tag{4.1}$$

$$x(n\Delta f) = \Delta f \sum_{m=0}^{N/2} X(m\Delta t) e^{i2\Pi m\Delta f n\Delta t} \tag{4.2}$$

Here $n = 0, 1, 2, 3, \ldots\ldots\infty$ and $m = 0, 1, 2, 3, \ldots\ldots(N-1)$

Block size (no. of samples): $N = T / \Delta t$ (4.3)

Frequency range (Hertz): $F_{\max} = 1/2\Delta t = \Delta f (N/2)$ (4.4)

Sampling rate (Hertz): $1/\Delta t = 2F_{\max}$ (4.5)

Frequency resolution (Hertz) : $\Delta f = 1/T$ (4.6)

Record length (Seconds) : $T = 1/\Delta f = N\Delta t$ (4.7)

The DFT, and thus any other quantities derived thereafter, is susceptible to Aliasing, which arises when the signal *x(t)* contains frequency components or "energy" above F_{max} of the DFT. Owing to the sampling or digitizing process, this energy will appear to be within the DFT frequency range. To avoid this, either F_{max} must be large enough to include all significant frequency components of *x(t)* or, for a given F_{max}, the components above F_{max} must be removed by analog filtering before sampling.

4.1.2 Spectral Density

Power Spectral Density (PSD), also called *Auto Spectral Density* $G_{xx}(f)$, and describes the frequency or spectral properties of a single time history [2, 16, 17, 18]. The *cross spectral density* $G_{xy}(f)$, describes the joint spectral properties of two time histories.

$$G_{xx}(f) = S_x(f)S_x{}^*(f) = |S_x(f)|^2 \quad (4.9)$$

$$G_{xy}(f) = S_x(f)S_y{}^*(f) \quad (4.10)$$

Here $S_x(f)$ is the two sided spectrum and $S_x{}^*(f)$ is the complex conjugate of $S_x(f)$. $G_{xx}(f)$ is the one sided spectral density.

4.1.3 Spectral Density-Correlation Functions

The correlation function of two random time records is a measure of how predictable, on average; one is at any instant from a measurement of the other at the same instant [2, 16, 17, 18]. It is obtained, in theory, by time shifting and multiplying the two variables together and integrating over all time. Correlation on a single time history is known as autocorrelation.

As seen in section 4.1.2, the spectral density functions $G_{xx}(f)$ and $G_{xy}(f)$ describe signal characteristics in the frequency domain, whereas the correlation functions $R_{xx}(f)$ and $R_{xy}(f)$ describe signal characteristics in the time domain. They are related through the Fourier transformation as follows.

$$\text{Autocorrelation}: G_{xx}(f) = 2\int_{-\infty}^{\infty} R_{xx}(\tau)e^{-i2\pi f\tau}d\tau \qquad 0 \le f < \infty \qquad (4.11)$$

$$R_{xx}(\tau) = 1/2\int_{-\infty}^{\infty} G_{xx}(f)e^{i2\pi f\tau}df \qquad -\infty < \tau < \infty \qquad (4.12)$$

$$\text{Crosscorrelation}: 2\int_{-\infty}^{\infty} R_{xy}(\tau)e^{-i2\pi f\tau}d\tau \qquad 0 \le f < \infty \qquad (4.13)$$

$$R_{xy}(\tau) = 2\int_{-\infty}^{\infty} G_{xy}(f)e^{i2\pi f\tau}df \qquad -\infty < \tau < \infty \qquad (4.14)$$

Correlation analysis is concerned with stationary processes. Thus in vibration analysis, it is usually carried out on a short interval of record during which physical parameters are assumed unchanged. Correlation techniques are used for detecting and

analyzing a weak signal in the presence of noise. They can also determine the contribution of each of several independent sources of excitation to a single output [2, 3].

4.1.4 Frequency Response Functions

Transfer functions are the Laplace transforms of a Single Input Single Output (SISO) linear dynamic system. The frequency response of a linear SISO system, *H(f)*, is easily obtained from the transfer function by replacing the Laplace operator, *s*, with the Fourier operator, *jw (w=2*pi*f)*. The relationship between the input and output or response of a linear system is shown in Figure 4.2. The complex transfer function *H(f)* describes the magnitude and phase of the response per unit sinusoidal input as a function of the input frequency.

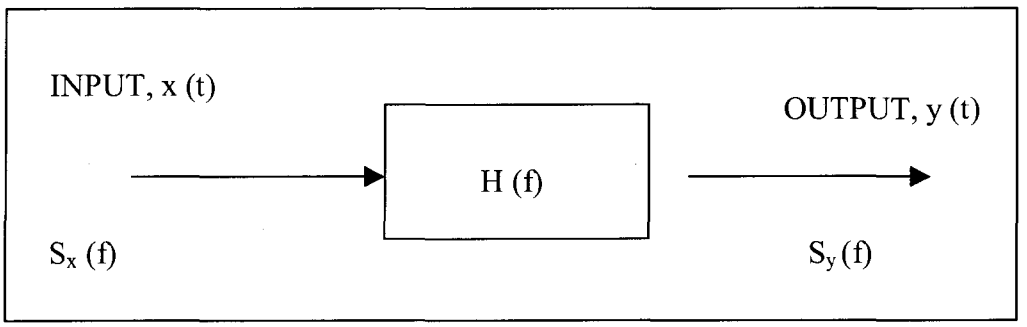

Figure4-2: Linear SISO System

Transfer functions can also be determined from the Fourier transforms of the input and response time-histories and from the spectral densities of the input and response signals when the input is a random process. The governing relationships [2, 16, 17, 18] are:

Fourier transforms: $$H(f) = \frac{S_y(f)}{S_x(f)} \tag{4.15}$$

Auto spectral densities: $$|H(f)|^2 = \frac{G_{yy}(f)}{G_{xx}(f)} \tag{4.16}$$

Cross spectral densities: $$H(f) = \frac{G_{yx}(f)}{G_{xx}(f)} \tag{4.17}$$

4.1.5 Coherence Function

The coherence function is a measure of the quality of the input, response and cross-spectral densities for a system as shown in Figure 4.2

$$\gamma_{xy}^{\ 2}(f) = \frac{|G_{xy}(f)|^2}{G_{xx}(f)G_{yy}(f)} \tag{4.18}$$

From eq. 4.16 and 4.17

$$\gamma_{xy}^{\ 2}(f) = \frac{|G_{xx}(f)H(f)|^2}{G_{xx}(f)|H(f)|^2 G_{xx}(f)} = 1 \tag{4.19}$$

The value of $\gamma_{xy}^{\ 2}$ is less than unity in practical cases. A coherence < 1 indicates that the response is not entirely attributable to the input alone, but may also be due to, for example, to extraneous noise and/ or nonlinearity of the system. In the frequency domain, the coherence function is analogous to the correlation coefficient in the time domain.

4.2 Spectral Density Matrix and Impedance Matrix

The Multi Input Multi Output (MIMO) Random Vibration Controller simulates environments that can be characterized by a reference spectral density matrix$[R(f)]$. Its objective is to find a set of drive signals for the actuators of the system-under-test, such that its response has a spectral density matrix which agrees with$[R(f)]$ [2, 3, 12, 19, 20]. The difference between the measured control signals and the reference signals is termed as control error signals.

System Identification is an important aspect of MIMO random control. This is done by actuating the system with drive signals that are band-limited and uncorrelated. The drive signals and the output signals are collected and stored as shown in Figure 4-3. The transfer function of the system is computed using this stored data. From equation 4.17:

$$[G_{cd}(f)] = [H(f)][G_{dd}(f)] \tag{4.20}$$

$$[H(f)] = [G_{cd}(f)][G_{dd}(f)]^{-1} \tag{4.21}$$

Here $[G_{cd}(f)]$ is the cross spectral density matrix between the output signals and the drive signals, and $[G_{dd}(f)]$is the auto spectral density matrix of the input signals. The inverse matrix of $[H(f)]$, $[Z(f)]$ is termed *Impedance matrix.* It allows the control system to determine the relative contribution of the control errors to each actuator's drive signal.

The initial drive signal is estimated using the prescribed reference signal$[R(f)]$ instead of the control signal. This is as shown in equations 4.22, 4.23 and 4.24.

$$[G_{cc}(f)] = [H(f)][G_{dd}(f)][H(f)]^{T*} \tag{4.22}$$

$$[G_{dd}(f)] = [H(f)]^{-1}[G_{cc}(f)][H(f)]^{-T^*} \quad (4.23)$$

$$[G_{dd}(f)] = [H(f)]^{-1}[G_{RR}(f)][H(f)]^{-T^*} \quad (4.24)$$

Above, the asterisk $[]^{T^*}$ denotes the complex conjugate transpose of a matrix. The drive signal amplitudes are iteratively calculated to minimize the error between the reference and the control.

The elements of the spectral density matrix elements are ordinary power spectral densities (PSDs) and cross-spectral densities (CSDs) as described in section 4.1.2. The PSDs are the diagonal elements, describing the power at each of the control points. The CSDs represent the coherence and phase between each of the control points, i.e. the spatial and frequency domain representation of the motion of the multiple control points [2, 12, 13, 16, 17, 18, 19].

4.3 Test Methodology

The Spectral Dynamics Jaguar controller is capable of generating random signal multi-axes drive functions. The controller principle is as discussed in section 4.2. This is again illustrated in Figure 4.3 [17].

Referring to Fig. 4-3, the data logger connected to the Jaguar controller records the time histories of both the input (Current ~ Force) termed as the drive signal ($d_1 \ldots . d_n$) and output signals (accelerometer readings at the chosen locations) also referred to as the control signal ($c_1 \ldots . c_n$) from the TEAM electrodynamic shaker. The recorded input (drive) signals' time histories were then applied as input signals to the FEA model at

UNLV. The recorded output time histories, as well as the PSDs computed by the Jaguar controller, were compared with the FEA output time histories and PSDs.

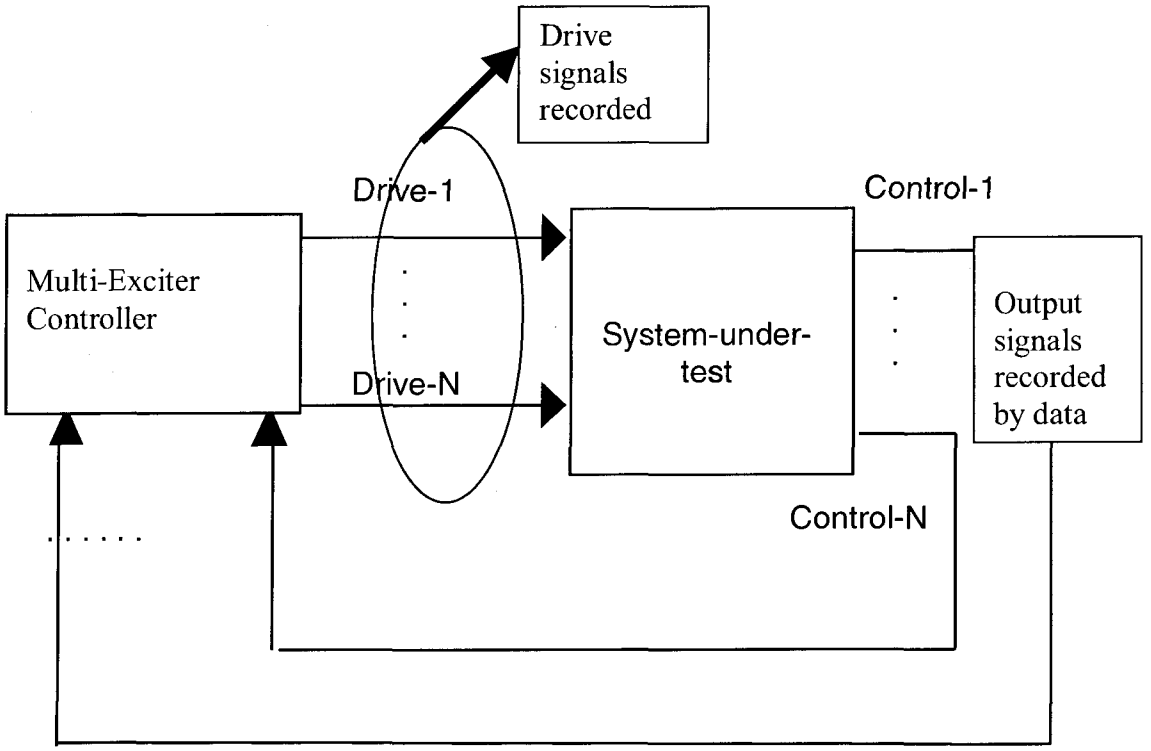

Figure 4-3: Spectral Dynamics Controller Concept

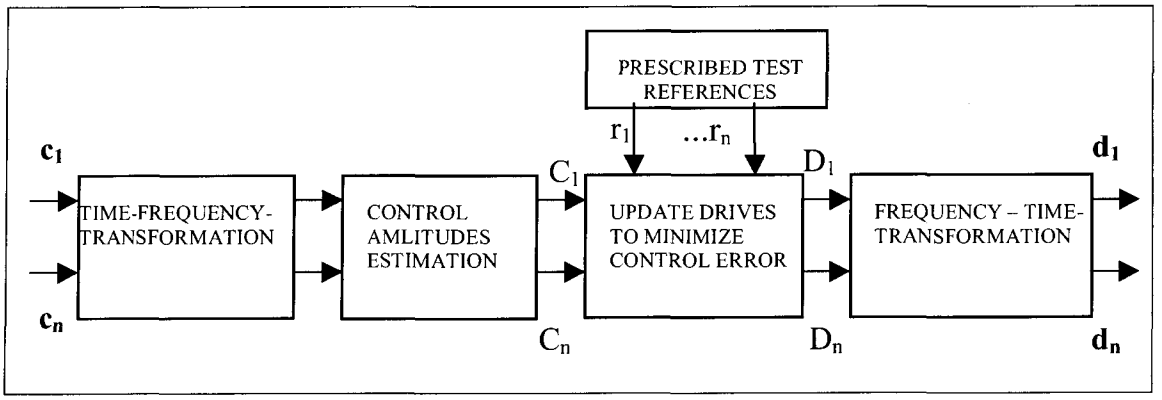

Figure 4-4: Spectral Dynamics Controller Block Diagram

Figure 4-4 depicts the basic working the Spectral Dynamics controller, Jaguar [20]. This block is a part of Figure 4-3. In the sense that the input and output signals collected by the data logger are processed in this block to compute the drive signals. Control vectors c_1, c_2, $c_3 \ldots c_n$ and drive signals d_1, d_2, $d_3 \ldots d_n$ are fed to a *time-frequency-transformation* block. This block produces the auto spectral density matrix $[G_{dd}(f)]$ and cross spectral density matrix $[G_{cd}(f)]$. Then the system-under-test is characterized by computing the transfer function matrix $[H(f)]$ [19, 20].

4.4 Reference Signals

Referring to Fig. 4-4, the set of 'prescribed test references' would be logically derived from MIL-STD 810F, METHOD 514.5. Among the spectra listed in MIL-STD 810F, METHOD 514.5, those extending to frequencies to 2 kHz are of the highest interest, since 2 kHz is generally accepted as the highest frequency of mechanically transmitted vibrations. PD spectra listed in MIL-STD 810F, METHOD 514.5 characterize uniaxial test regimes. Fig. 4-5 shows one PSD spectra from MIL-STD 810F, METHOD 514.5 [4]. This is the type of vibration experienced by Jet aircraft store equipment.

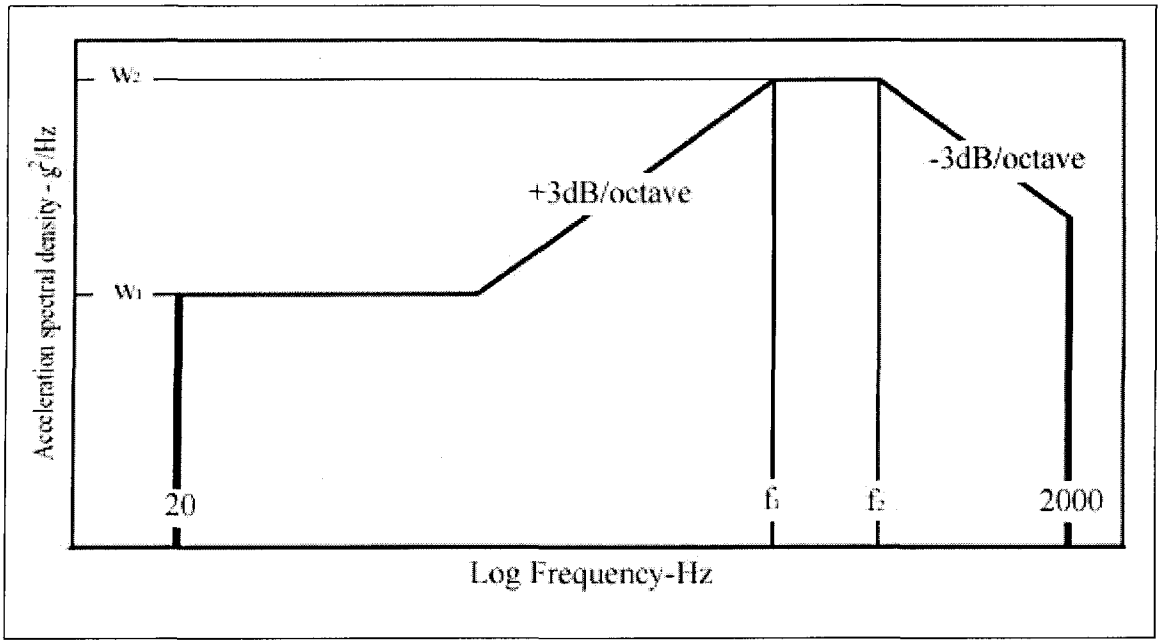

Figure 4-5: Sample PD Spectra from MIL-STD 810F [4]

4.5 Sensor Placement

Tri-axial accelerometers were strategically placed at 16 different locations on the center member to record the data. These locations were carefully chosen following several experiments at Team Corp., to control the original table through the 1200 Hz resonance. The 'stick-model' of Figure 4-6 lists locations for sensor placement.

Referring to table 4-1, signal streams are labeled according to accelerometer location, direction and orientation based on the global frame xyz. The numbers 1-16 denote location points according to the stick model of Figure 4-6. Points 1, 2, and 3 denote points on the bottom shoulder of the center member. Points 5, 6, and 7 are located on the top shoulder of the center member. Point 4 is in the middle of the vertical section. Points 8 through 16 are on the table top of the center member.

The orientation of each triaxial accelerometer varies with the orientation of the surface onto which it is mounted. The orientation of a particular output signal is characterized in Table 4-1 relative to the global X-Y-Z frame shown at the bottom right corner of Figure 4-6. Sensor orientation is expressed as + when consistent with the global X-Y-Z frame, and as – otherwise. For example, the upward directed signal at point 3 is expressed as 3Z+.

Drive inputs are applied to points 1Z+ (z1), 2Y- (y1), 3Z+ (z2), 5X+ (x1), 7X+ (x2) and 7Y- (y2). Two drive signals (x1, x2), (y1, y2), and (z1, z2) are averaged to calculate the frequency response with respect to the outputs. This is explained in section 4.6. Table 4-1 shows each point and the actuator location and orientation.

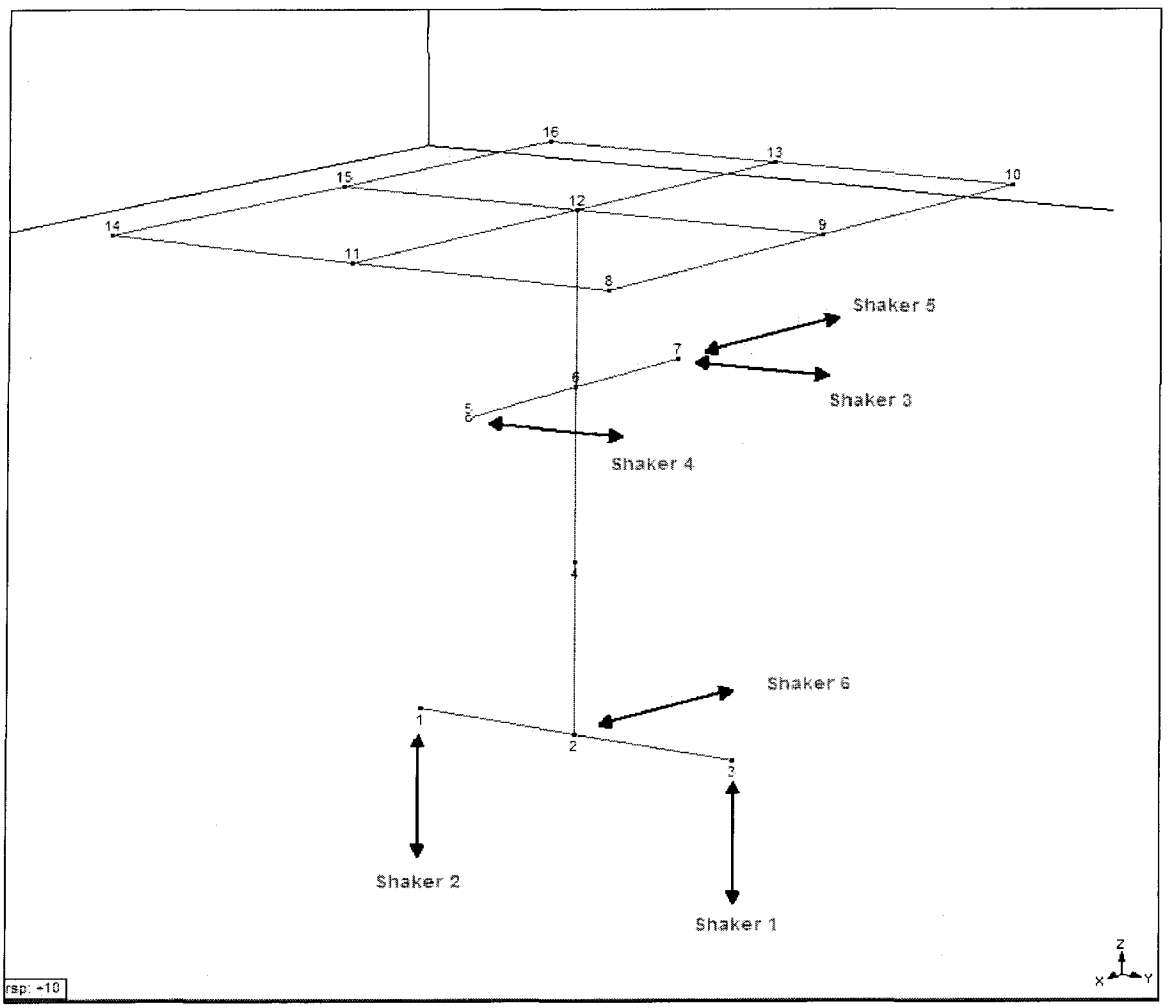

Figure 4-6: Sensor Locations

Table 4-1: Actuator Location and Orientation

Drive#	Orientation
1	3Z+
2	1Z+
3	7Y+
4	5Y-
5	2X+
6	7X+

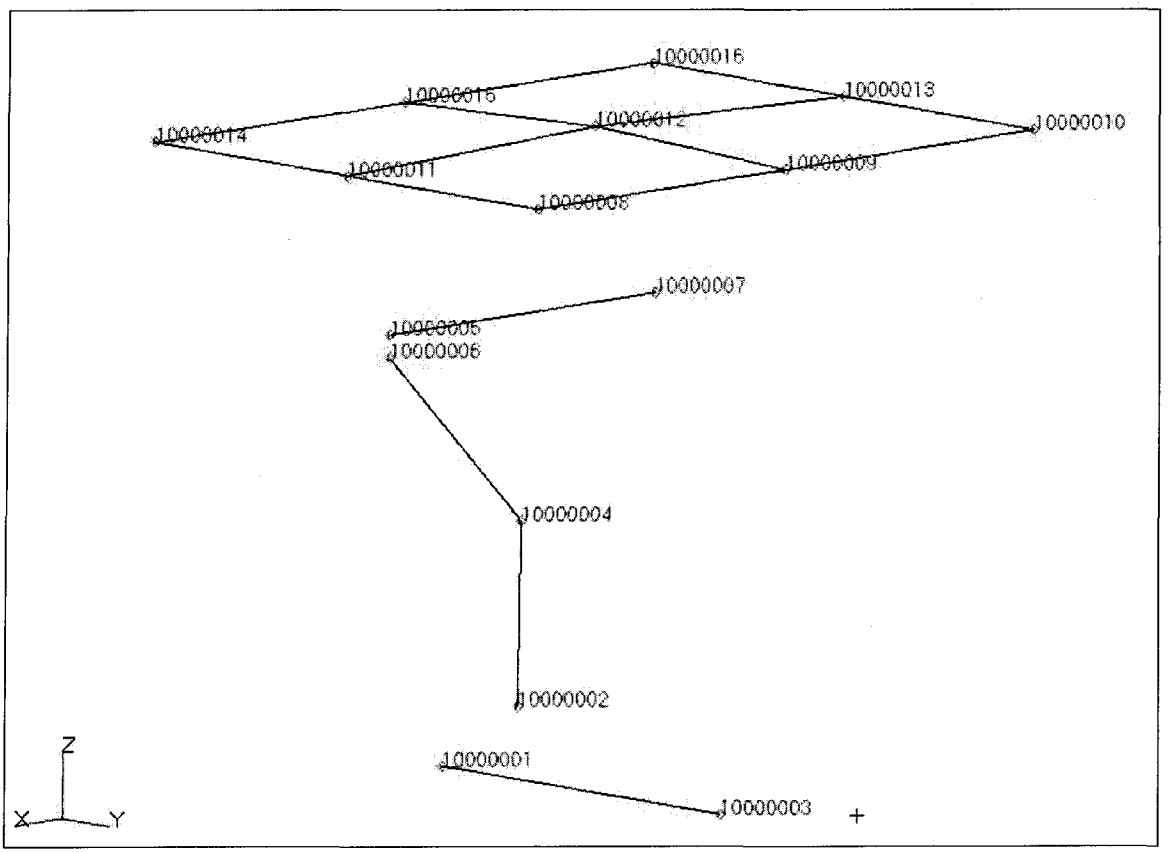

Figure 4-7: Sensor Locations in FE Model

4.6 Single-Axis and MIMO Testing

The primary objective of the test program was to determine the modal characteristics as well as the frequency response of the shaker system and to compare predictions from the finite element model against these experimental test results. The difference between both permits validation of the accuracy of the finite element model.

The structural analysis consisted of modal analysis and various vibration testing experiments single frequency single exciter tests, followed by single axis two exciter tests, two axes sinusoidal excitation tests and six axes excitation tests. These are discussed in the following sections.

4.6.1 Modal Analysis

Modal tests, also known as ground vibration tests in the aircraft industry, are tests conducted to determine experimentally the natural frequencies, mode shapes, and associated damping factors of a structure [2, 3, 6, 21, 22, 23].

For linear systems, the modes also result as the roots of the characteristic equation of the mathematical model of any given system. Consider a single DOF spring-damper-mass system. The general mathematical model of this system is shown in equation 4.26

$$m\ddot{y}(t) + c\dot{y}(t) + ky(t) = u(t) \tag{4.26}$$

Where m = mass constant, c = damping constant, k = stiffness constant and $u(t)$ is the input force. $\ddot{y}(t) = d^2y(t)/dt^2$ and $\dot{y}(t) = dy(t)/dt$ are acceleration, velocity and displacement.

The Laplace transform of this differential equation is called the characteristic equation and is given by:

$$ms^2 + cs + k = 0 \tag{4.27}$$

The roots of this equation give us the modal information about the system under consideration.

$$\lambda_1 = -\sigma_1 + j\omega \quad \text{and} \quad \lambda_2 = -\sigma_2 + j\omega \tag{4.28}$$

λ_1 and λ_2 are called the modes, σ_1 is the damping factor for mode 1 and ω is the undamped natural frequency for mode 1. $\lambda_2 = -\sigma_2 + j\omega$ is usually the complex conjugate of λ_1.

The system of equation 4.26 can also be represented using state space equations. Let select the displacement and velocity as the state variable; that is, $x_1 = y$ and $x_2 = \dot{y}$. Then

we have, $\dot{x}_1 = x_2$ and $m\dot{x}_2 = u - cx_2 - kx_1$. This can be represented as a state-space equation as shown:

$$\begin{bmatrix} \dot{x}_1(t) \\ \dot{x}_2(t) \end{bmatrix} = \begin{bmatrix} 0 & 1 \\ -k/m & -c/m \end{bmatrix} \begin{bmatrix} x_1(t) \\ x_2(t) \end{bmatrix} + \begin{bmatrix} 0 \\ 1/m \end{bmatrix} u(t) \tag{4.29}$$

$$y(t) = \begin{bmatrix} 1 & 0 \end{bmatrix} \begin{bmatrix} x_1(t) \\ x_2(t) \end{bmatrix} \tag{4.30}$$

Generally, a linear time invariant system can be represented as a state space equation of the form

$$\dot{x}(t) = Ax(t) + Bu(t) \tag{4.31}$$

$$y(t) = Cx(t) + Du(t) \tag{4.32}$$

Here A is called the mass matrix and $\det(\lambda I - A) = 0$ is the characteristic equation. The solution to the homogeneous equation also gives us the modes λ_1 and λ_2 also known as the eigenvalues [21, 22, 23].

Experimentally, the modes are found by exciting the system with sinusoidal or transient excitation at a number of points of the structure. The responses at locations throughout the structure then define the mode shape for that frequency. The methodology and results of modal analysis are discussed in chapter 5.

4.6.2 Six-Axis Testing

Accelerometer signals at points 1, 3, 4, 8, 12, 13 and 14 have been recorded. X, Y and Z are output signal coordinates. Table 4-2 shows each point and the accelerometer location and orientation.

Table 4-2: Accelerometer Location and Orientation

Point	X	Y	Z
1	+3	-1	+2
3	+1	+2	-3
4	+3	+2	+1
8	+2	+1	+3
12	+2	+1	+3
13	+2	+1	+3
14	+2	+1	+3

We apply spectral output reference definitions as per MIL-STD 810F analogous to Fig. 4-5 to each driven coordinate. In each of the cases listed in table 4-5, the input/output time histories, in turn the shaker system performance and coherence were recorded after the Jaguar controller had modified the 'drives' such that the spectrum of each observed I/O pair was within the specified bounds, of say +/- 3dB deviation from the specified reference.

In order to make reasonable comparison between the experiments and simulations, the time domain input functions applied to the TEAM Tensor during experiments were recorded with a sampling rate of 0.09775 10,230 kHz. These input functions included sine as well as random signals. These recorded inputs were then applied to the FE model for the simulation purposes. Time domain output responses were recorded and statistically compared.

Table 4.3 describes the experiments conducted at TEAM, and the corresponding FEA performed at UNLV. Accelerometers are installed at points 1, 3, 4, 8, 12, 13 and 14. X, Y

and Z are output signal coordinates. Table 4-2 shows each point and the accelerometer location and orientation.

First column of Table 4-3 shows the drive locations, which are actuators that were active for that particular set of experiment, the test type, which could be any of the following: single input, single axis, and dual input, dual axis, and six inputs, three axis. Within these experiments, the input could have been Sine or Random. The third column shows the accelerometer locations where data were collected. These experiments and their respective results are discussed in chapter 5.

Table 4-3: List of Tests Conducted on Modified Team Shaker Platform

Drive locations	Test Type	Accelerometer Locations	Responsible
1, or 3, or 5, or 7	Single Input • Random (30 to 3,000 Hz) • Sine sweep 300 to 3,000 Hz • Sine input at 1 kHz, 1.6 kHz, 2,050 Hz	Points 1 through 7, point 12, and two sides of table, e.g. points 8, 11, 14 through 16.	TEAM
1 and 3, in phase & out of phase (0, 90, & 180 degrees)	Dual input • Random (30 to 3,000 Hz) • Sine sweep 300 to 3,000 Hz • Sine input at 1 kHz, 1.6 kHz, 2,050 Hz (excite both (z-axis) voice coils)	Points 1 through 7, point 12, and two sides of table, e.g. points 8, 11, 14 through 16.	TEAM
All Shakers	Six-axis translation Random (30 to 3,000 Hz) no coherence	Points 1 through 4, point 12, and two sides of table, e.g. points 8, 11, 14 through 16.	TEAM & UNLV
All Shakers	Controlled Tabletop Six-axis translation Random (30 to 3,000 Hz) no coherence	Points 8, 13, 14	TEAM & UNLV

4.7 Mathematical Analysis of Experimental Data

4.7.1 Transfer Function: Translations & Rotations

The relationship between drives and outputs are as shown in the transfer function matrix in Figure 4-7, they are consistent with Marcos Underwood's publication, [8]. This method is briefly discussed in chapter 1 on page 5 of this publication.

There are 6 input signals and there are 6 outputs (3 translations and 3 rotations). The contribution of each input to each output should be determined first in order to obtain the transfer functions.

Translation in each direction (X, Y, and Z) will result mainly due to the inputs in the same direction.

The rotations (roll, pitch and yaw) are function of the forces in the perpendicular directions. Referring to Figure 4-8, the inertial mass is accelerated at points A and B, with R being the distance between A and B. The angular acceleration of the mass is the difference of accelerations at points A and B divided by the distance R.

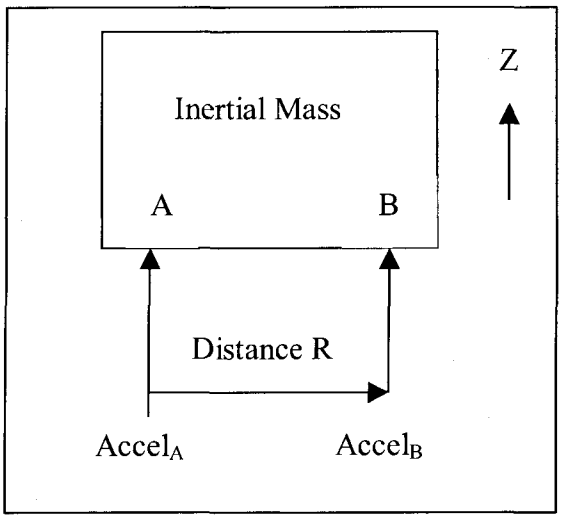

Figure 4-8: Rotational Components

Figure 4-9 shows the table top. The points of interest are 8, 13, and 14. Accelerometer measurements were recorded at these three locations in the following coordinate directions: 8z (Z2), 13x (X), 13y (Y1), 13z (Z1), 14y (Y2), and 14z (Z3). Using these acceleration data, the rotational component is calculated as described above in Figure 4-8.

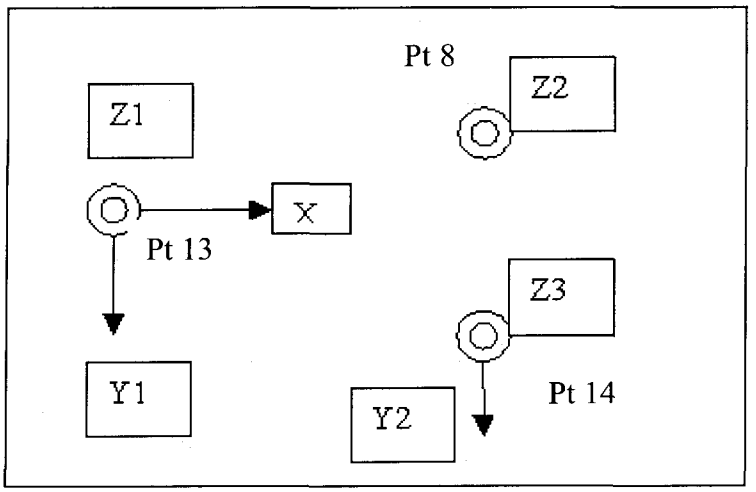

Figure 4-9: Sensor Locations and Orientations for 6-Axis Control

$$\begin{pmatrix} X \\ Y \\ Z \\ R_X \\ R_Y \\ R_Z \end{pmatrix} = \begin{bmatrix} 1 & 0 & 0 & 0 & 0 & 0 \\ 0 & 0.5 & 0.5 & 0 & 0 & 0 \\ 0 & 0 & 0 & 0.33 & 0.33 & 0.33 \\ 0 & 0 & 0 & 0 & 0.1538 & -0.1538 \\ 0 & 0 & 0 & 0.1076 & 0 & -0.1076 \\ 0 & 0.1076 & -0.1076 & 0 & 0 & 0 \end{bmatrix} \begin{pmatrix} x \\ y_1 \\ y_2 \\ z_1 \\ z_2 \\ z_3 \end{pmatrix}$$

- The rotation about the X-axis is estimated from the difference in accelerations Z2 and Z1 due to the inputs 1z and 3z. Using the *Pythagoras theorem,* the distance between the two accelerometers at points 8 and 13 is approximately 9.29 inches. The distance between the two actuators at points 1 and 3 is 4 inches.
- The rotation about the Y-axis is estimated from the phase of the transfer function between Z3 and Z1, the inputs considered are 1z and 3z. The distance between the two accelerometers at points 13 and 14 is approximately 9.29 inches. The distance between the two actuators at points 1 and 3 is 4 inches.
- The rotation about the Z-axis is estimated from the phase of Y2 to Y1, the inputs considered are 5y and 7y. The distance between the two accelerometers at points 13 and 14 is approximately 9.29 inches. The distance between the two actuators at points 5 and 7 is 4 inches.

4.7.2 Data Analysis using MATLAB

The experimental data were recorded by TEAM as ASCII text files, listing the time histories of the input and output variables during the experiment. The records are imported to Excel worksheets, which are then loaded into MATLAB.

The plots in Figure 4-10 shows the raw and the filtered data obtained from both experiment and simulation. Standard Savitzky-Golay Matlab filtering functions were used reduce the noise. The frequency transforms employed Kaiser-Bessel windowing.

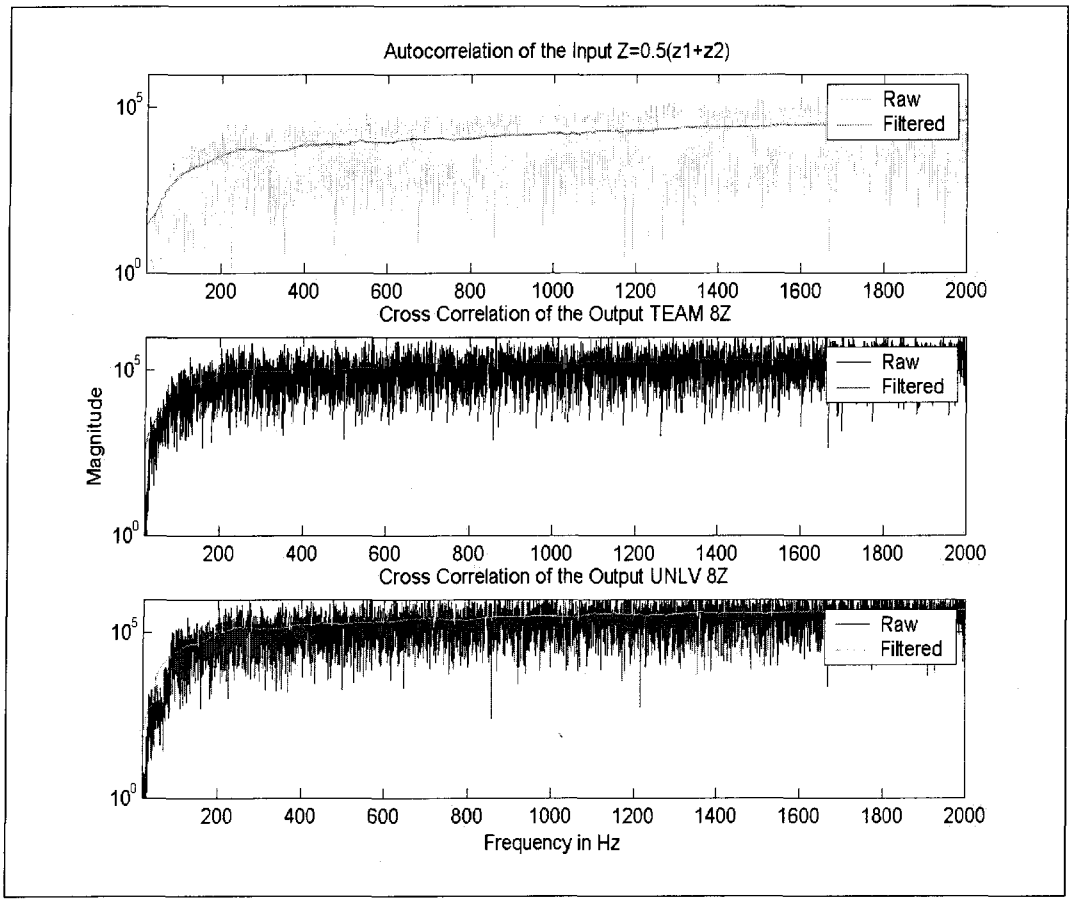

Figure 4-10: Raw and Filtered Data

Savitzky-Golay smoothing filters (also called digital smoothing polynomial filters or least-squares smoothing filters) "smooth out" a noisy signal whose frequency span (without noise) is large. In this type of application, Savitzky-Golay smoothing filters perform much better than standard averaging FIR filters, which tend to filter out a significant portion of the signal's high frequency content along with the noise. Savitzky-

Golay filters are optimal in the sense that they minimize the least-squares error in fitting a polynomial to frames of noisy data. The Matlab code to obtain the frequency response is shown below.

$$x : input$$
$$y : output$$
$$x1 = fft(autocorrelation(x))$$
$$y1 : fft(crosscorrelation(x, y))$$
$$frequencyresponse : \frac{y1}{x1}$$

'xcorr' estimates the auto-correlation and cross-correlation sequence of a random process. 'Y = fft(X)' returns the discrete Fourier transform (DFT) of vector X, computed with a fast Fourier transform (FFT) algorithm. If X is a matrix, fft returns the Fourier transform of each column of the matrix.

CHAPTER 5

RESULTS

5.1 Modal Analysis

Several experiments were conducted at the Team Corp in order to determine the dynamics and natural frequencies of the structure.

In a first series of experiments, both center members (original and modified) were excited using one exciter at a time, collecting 3-axis acceleration to drive force transfer functions at 16 locations on the center member and tabletop.

Figure 5.1 shows the frequency response of the original center member due to the single exciter testing. The frequency response at all the 16 points with respect to all the actuating points is overlaid in this graph.

Resonance is observed around 1200 Hz and 1500 Hz within the 2000 Hz bandwidth range of interest. The resonant frequencies move to 1600 Hz and 2000 Hz in the stiffened modified center member, see Figure 5-2.

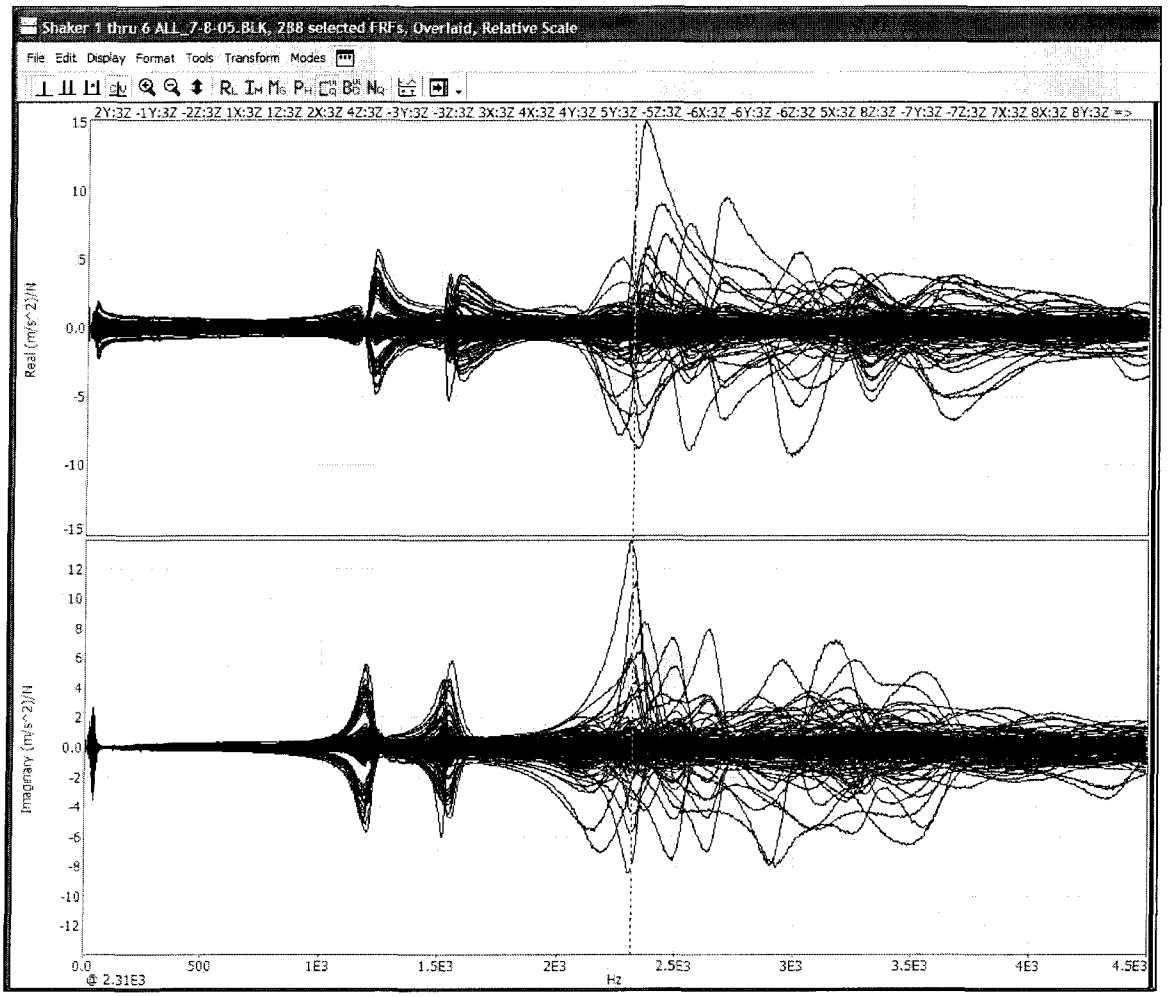

Figure 5-1: Collective Frequency Responses of the Original Center Member

The modified center member was excited with a broadband random signal using both vertical exciters simultaneously in phase. The frequency response at all the 16 points with respect to all the actuating points are overlaid and shown in Figure 5-2.

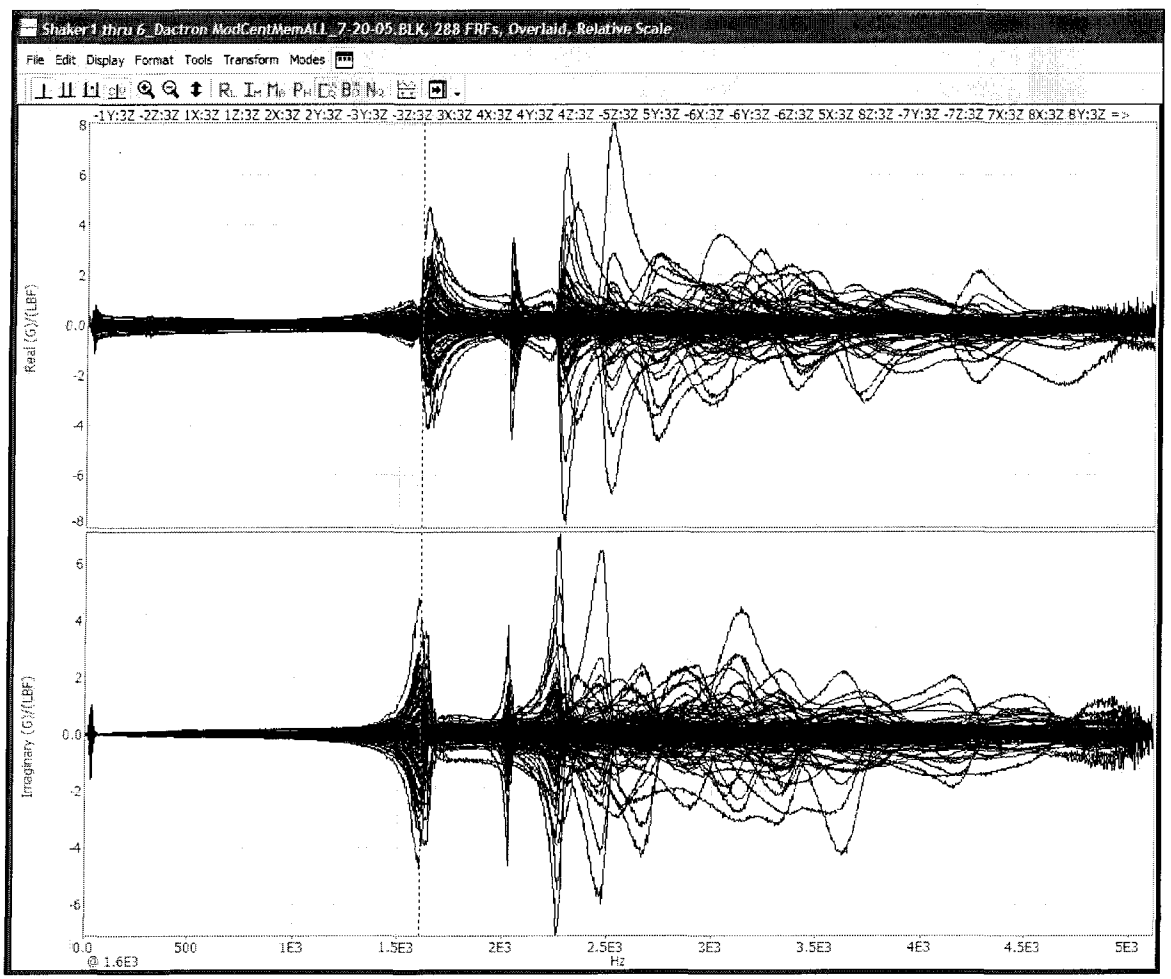

Figure 5-2: Collective Frequency Responses of the Modified Center Member

The data collected using simultaneous excitation by all 6 exciters, while controlling the power spectral density of 6 response accelerometers (which together form a linearly independent set of measurements suitable to define 6 degrees of freedom) turned out to be useless, due to suspicious data sets strewn throughout the data.

At UNLV, the MSC-NASTRAN modal analysis module computed the natural frequencies of the FE model. The FE model exhibits consistently higher resonance frequencies than the experimental observations. The results agree better when the number of elements is increased in the FE model, making the FE model 'softer'.

A comparison of experimentally recorded and computed modes for the original geometry is shown in table 5-1.

Table 5-1: Eigenfrequencies of Original Center Member

Mode #	Experiment Frequency	FEA Frequency	Description
1	1180	1230	Bending about X & Y at point 4
2	1520	1701	Torsion about Z, Bending about Y at point 4, Torsion & Bending about X at point 4

The results of modal analysis of the original center member suggested that the structure lacked stiffness. The center member was stiffened by making the vertical beam section solid, raising the resonant frequencies of the center member considerably. The result is shown in table 5-2.

Table 5-2: Eigenfrequencies of Modified Center Member

Mode #	Experiment Frequency	FEA Frequency	Description
1	1600	1617	Arms bending at joint with vertical CM
3	2020	2285 & 2398	Lower Arm bending about X

5.2 Six-Axis Random Testing

The center member was excited in all six axes with random input signal without any coherence. The resulting input and output time histories were recorded and stored on the Jaguar system's Throughput Disk (TPD).

The recorded 6-axis force-input time histories were applied to the MSC-Nastran FE model. Several delays were caused by the MSC-Nastran requirement to write very large scratch files to the hard drive. We added the largest hard drive available from Dell (160 GB capacity) and were able to extend the simulation to a reasonable time length.

As mentioned in Sections 4.2, 4.3 and 4.4, and 4.6, the Jaguar controller modifies the drive signals in order to obtain the output (control) signals within a error margin of +/- 3dB deviation from the specified reference. Thus it is sufficient for us to match the waveform shape in order to validate the finite element model.

Figures 5-3 to 5-5 show the frequency response of the system for random inputs at point 8. The graphs obtained for various other center member locations, namely points 1, 3 and 4, 12, 13, and 14 are shown in Appendix A. The Y axis magnitude of the frequency response in Figures 5-3 through 5-5 and Figures A1 through A18 is lbf/g and X axis scale is Hz.

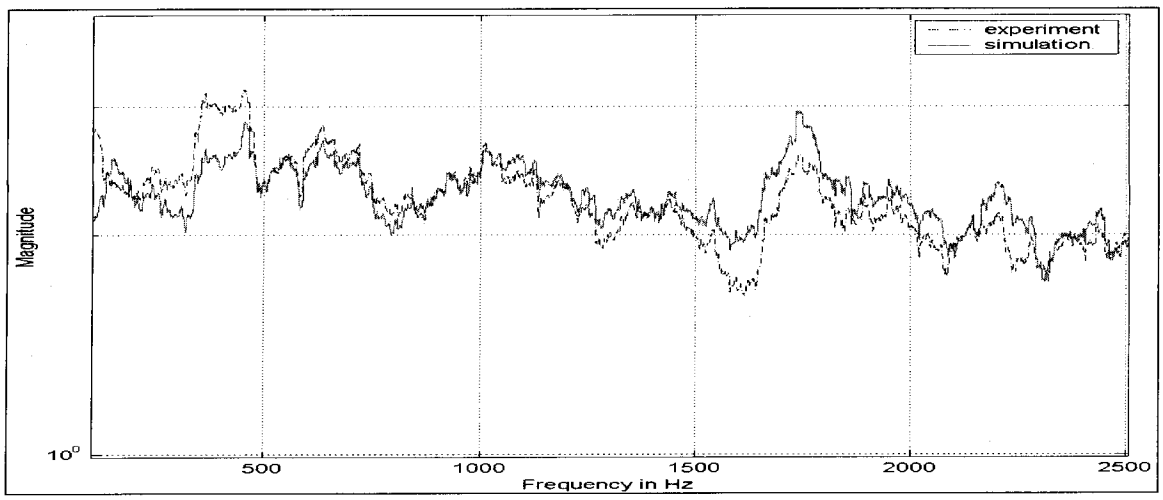

Figure 5-3: Frequency Response at Pt 8 in X Direction

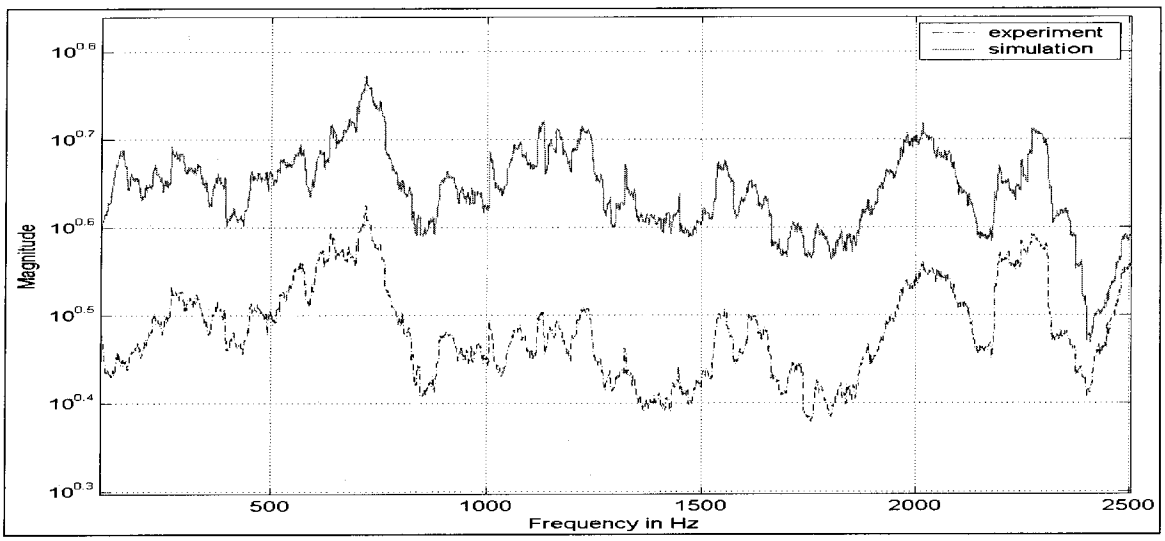

Figure 5-4: Frequency Response at Pt 8 in Y Direction

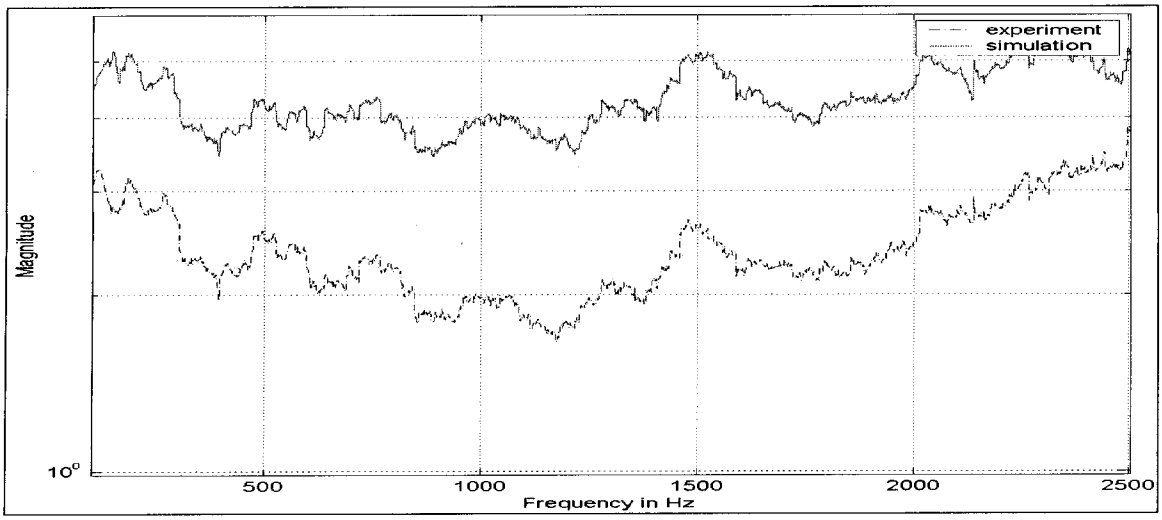

Figure 5-5: Frequency Response at Pt 8 in Z Direction

5.3 Six Axis Shaker Control

In one test, the shaker was actively controlled to maintain the table top flat over the entire frequency range to 2 kHz. The three reference locations are the Z-coordinates of points 8, 13, and 14. Six measurements points were chosen so as to obtain a 6-by-6 control matrix in the Jaguar Controller. The number of sensors can easily be increased by adding additional channels. The Jaguar Controller seeks to minimize the error between the reference and the recorded spectra. The controller updates the Z-matrix (see chapter 4.2) iteratively seeking the best possible agreement of the measured output at the reference locations with the reference spectra. The objective of the control experiment was to suppress the resonance within the frequency range of 0 Hz to 2000 Hz. The frequency responses of the controlled table top are shown below and it is evident that the objective was achieved.

Here the response is measured with respect to all the individual inputs. The graphs are labeled in a simple manner. For example, the frequency response at point 8 in the Z

direction due to excitation in the X direction is labeled as 8Z/X. This is seen in Figure 5-6. The main diagonal of the spectra is shown here. The rest of the frequency response curves are shown in Appendix B. The Y axis magnitude of the frequency response in Figures 5-6 through 5-12 and Figures B1 through B13 is lbf/g and X axis scale frequency is Hz.

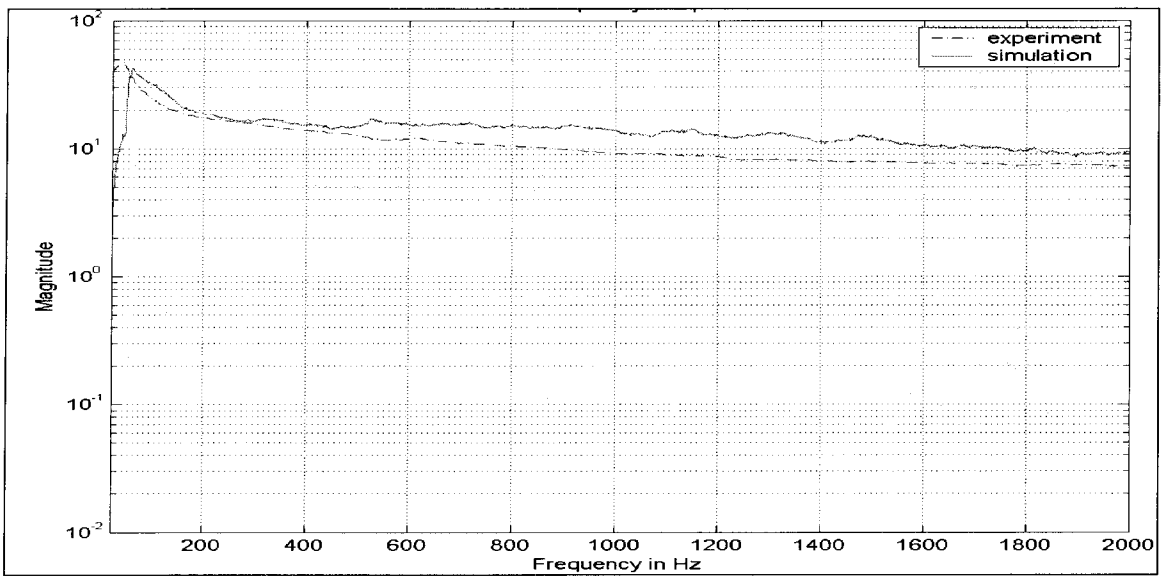

Figure 5-6: 8Z / Z

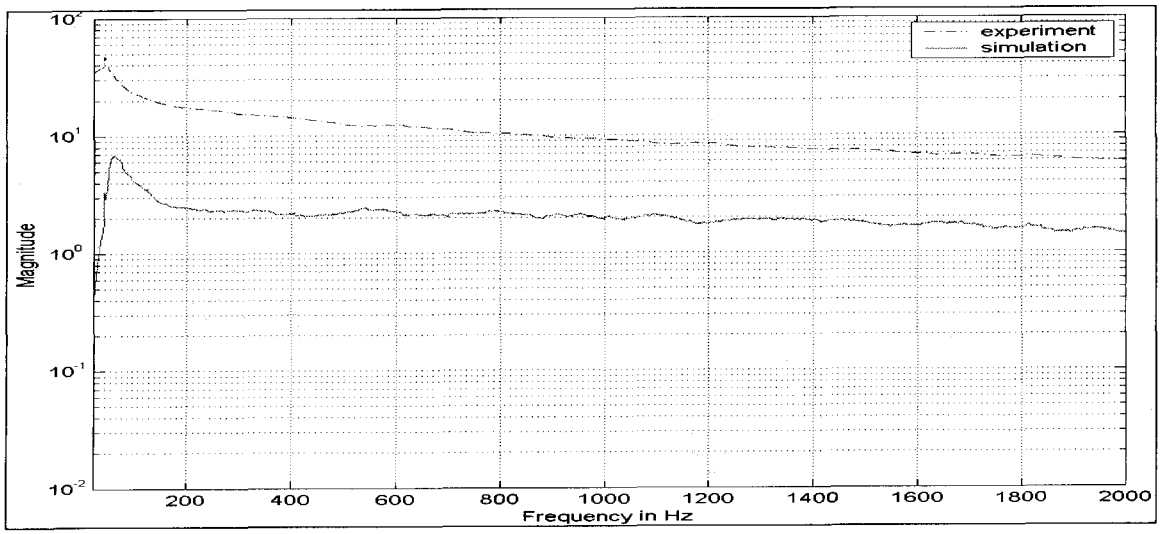

Figure 5-7: 13X / X

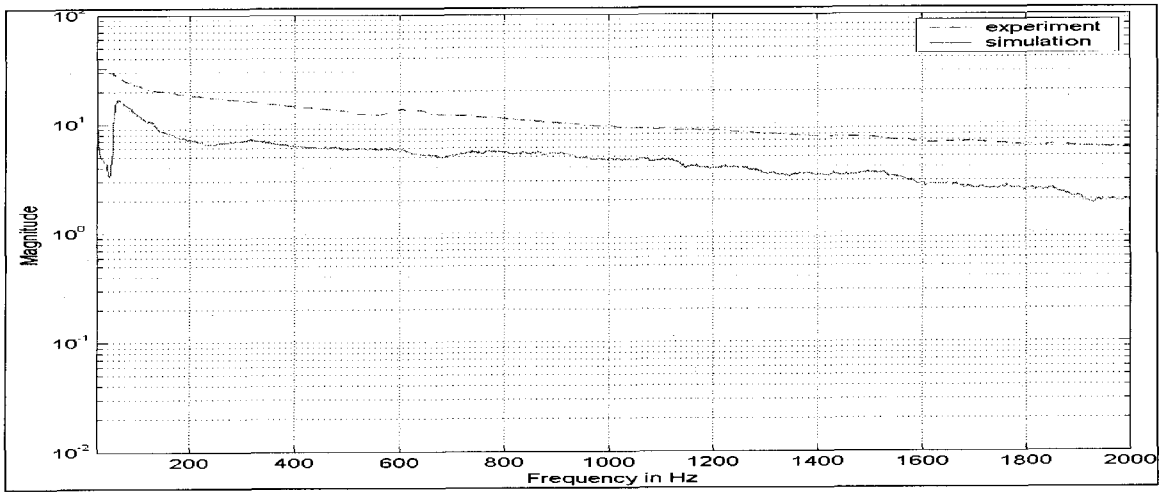

Figure 5-8: 13Y / Y

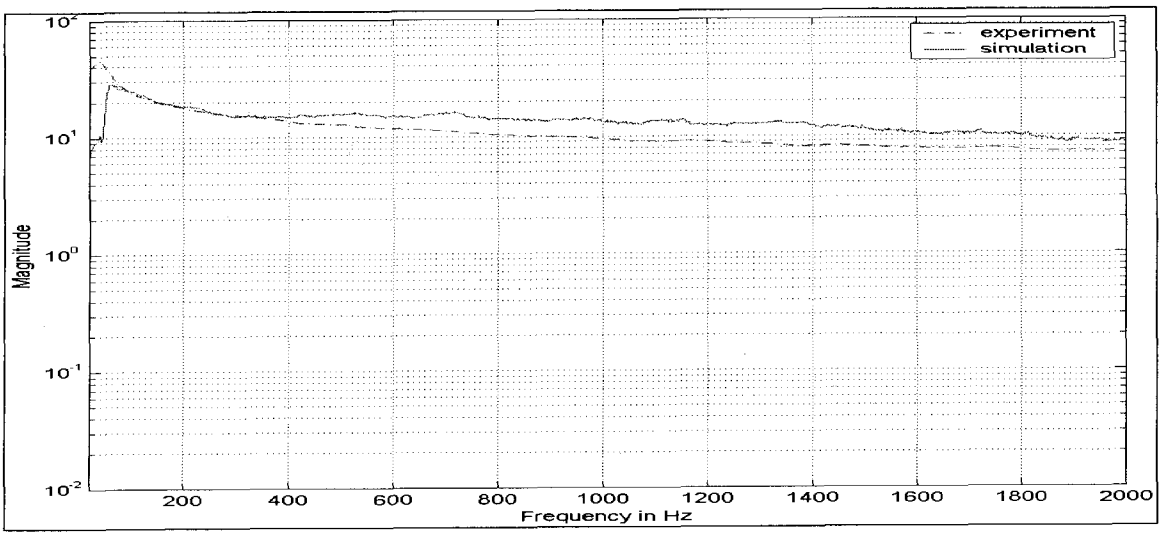

Figure 5-9: 13Z / Z

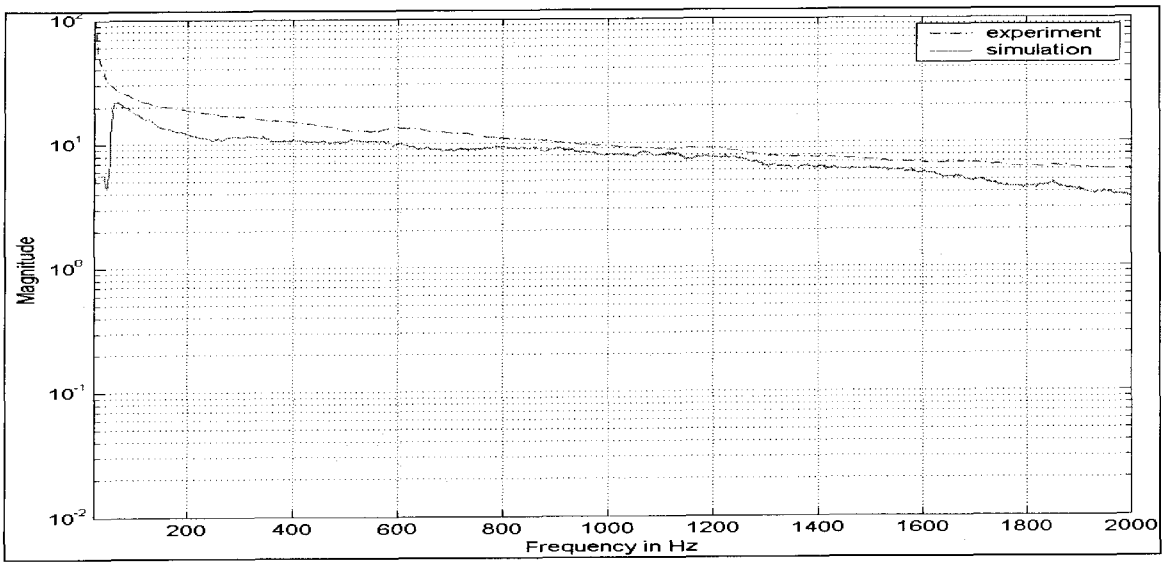

Figure 5-10: 14Y / Y

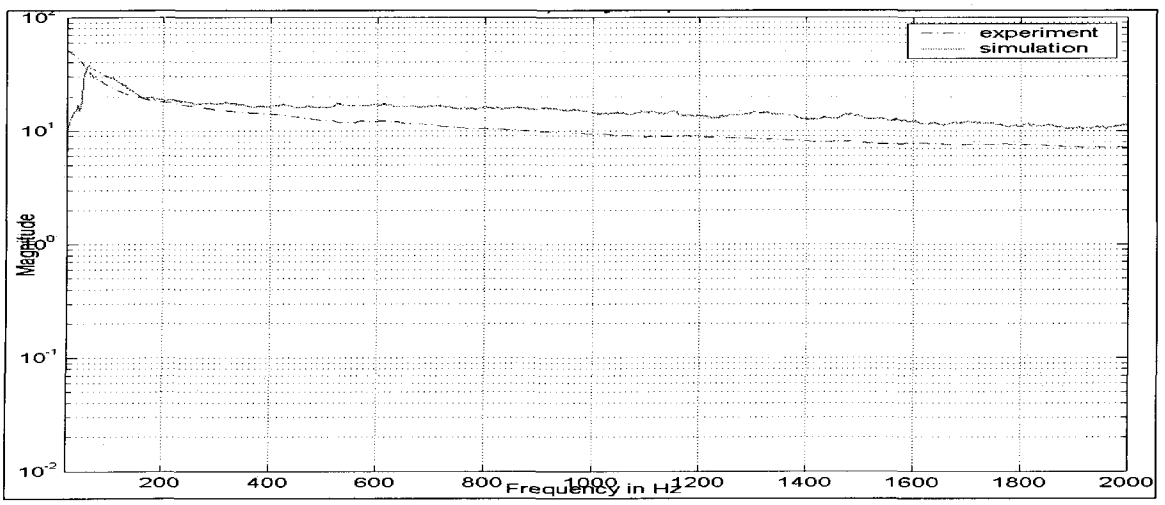

Figure 5-11: 14Z / Z

It is evident that though there is a difference in magnitudes, the frequency response curve obtained experimentally is replicated with simulations.

5.4 Modal Analysis of Shaker with Attached Test Object

At UNLV, we ran simulations with a 2 pound steel block attached to the shaker table. This block acts as a test object. These experiments are not yet conducted at the TEAM Corporation to make any comparison. The input is the random drive signal from the six axis random experiment and the outputs were collected at 4 different points on the table top. They are 8, 12, 13 and 14. The modal analysis of the structure when a test object is attached to it is discussed below in Figure 5.40 and table 5.3. In the first set of data, the load is placed in the center of the table.

Table 5-3: Eigenfrequencies with the Test Object Attached at the Corner

Mode #	FEA Freq	Description
1	860.48	Table flapping at the point of attachment
2	1560.8	Torsion about X at point

In the second case the load is attached to the corner of the table top. It is noticed that the predicted resonant frequencies of the system vary, depending on the placement and mass of the attached load. This has to be verified experimentally.

Table 5-4: Test Object Attached to the Center

Mode #	FEA Freq	Description
1	761.45	Torsion about Z
2	1561	Bending about X at point 4
3	1020.2	Bending about Y at point 4
4	1497.6	Table top flapping
5	1531.6	Arms bending at joint with vertical CM

CHAPTER 6

CONCLUSIONS AND FUTURE WORK

6.1 Conclusions

The objective of the research effort described here is the predictive analysis of six-axis dynamic shaker designs, and the validation of the modeling and design concepts through experiments. Finite element analysis and spectral response analysis were used to compare FE model predictions and experimental results. Overall, good correlation between the experimentally measured and model computed frequency responses has been achieved.

6.2 Future Work

The test data indicate that more damping of the structural modes is very desirable in future systems. The Spectral Dynamics control system performed well in controlling the shaker system through its resonances. However, even with the good dynamic range of the control system, the resonance at about 1600Hz was not well controlled.

In the experiments, the drive current of the electrodynamic actuators was measured as a voltage differential across a small series resistor. Drive current is assumed to be proportional to the actuation force.

Measuring the current with a voltage drop across a resistor has potential problems. Hall Effect current sensors might offer better signal quality. Additional experiments are planned to characterize the controller and shaker system performance under various MIMO control scenarios.

APPENDIX A

SIX-AXIS RANDOM FREQUENCY RESPONSE

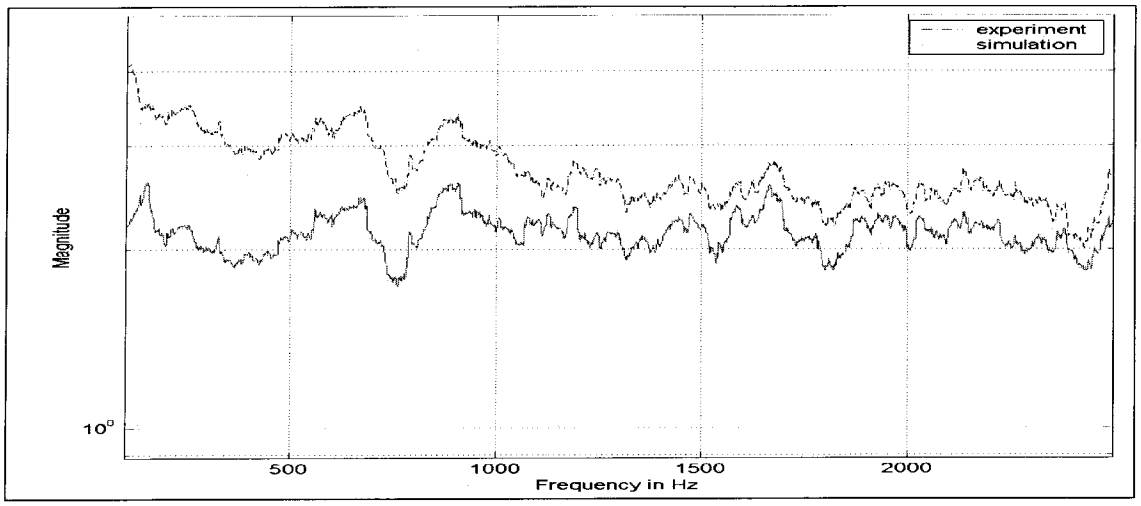

Figure A1: Frequency Response Spectrum at Point 1 in X Direction

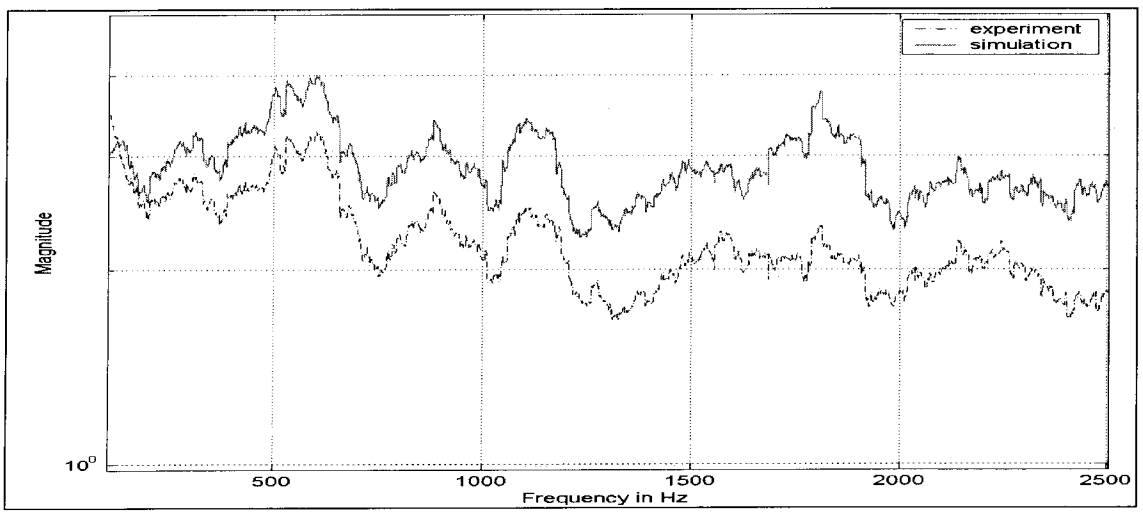

Figure A2: Frequency Response at Pt 1 in Y Direction

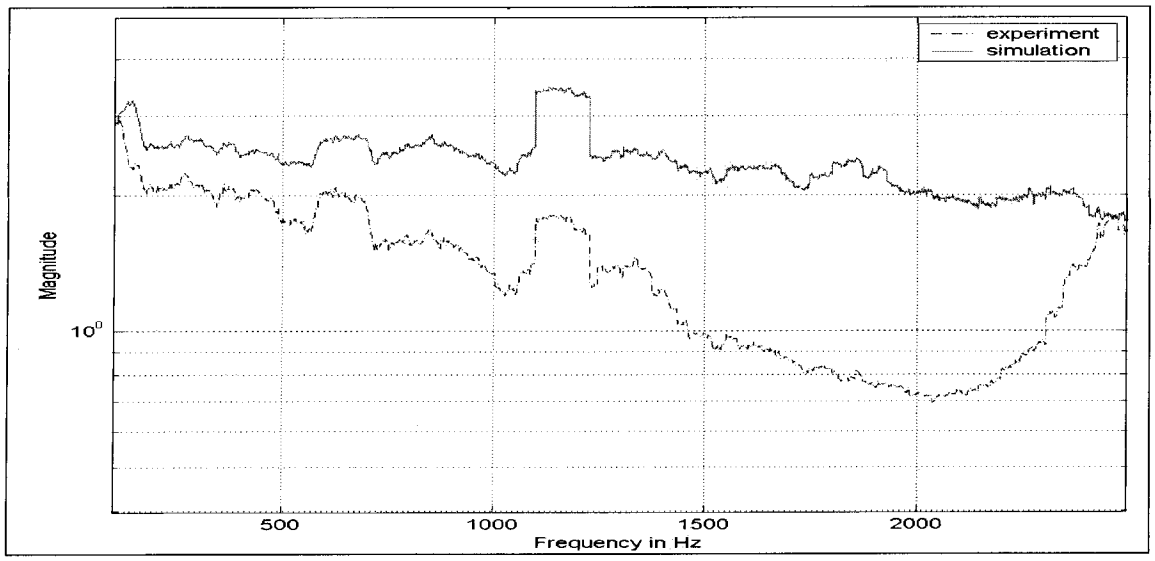

Figure A3: Frequency Response at Pt 1 in Z Direction

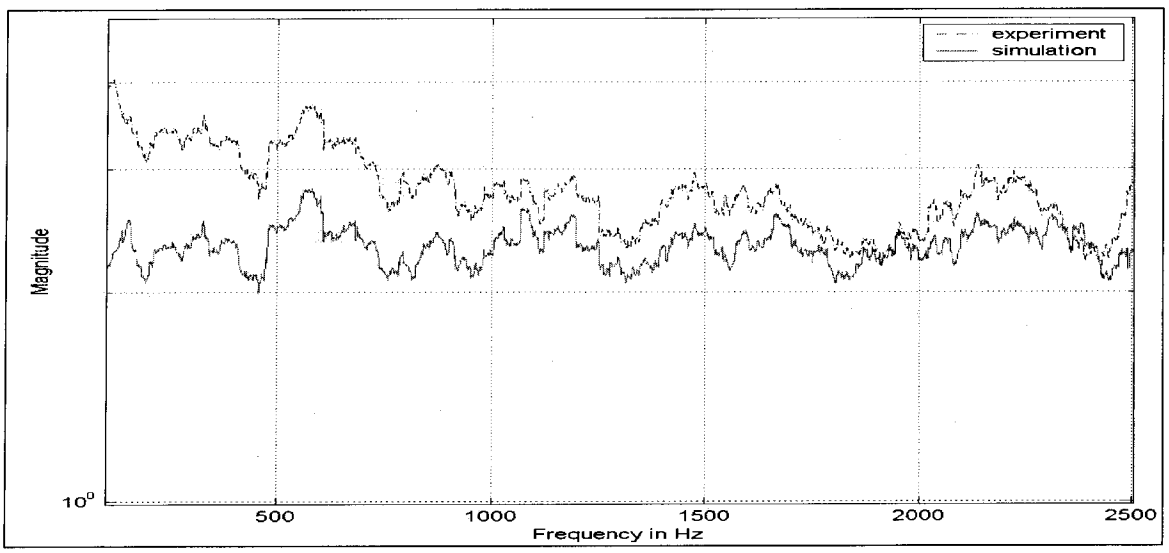

Figure A4: Frequency Response at Pt 3 in X Direction

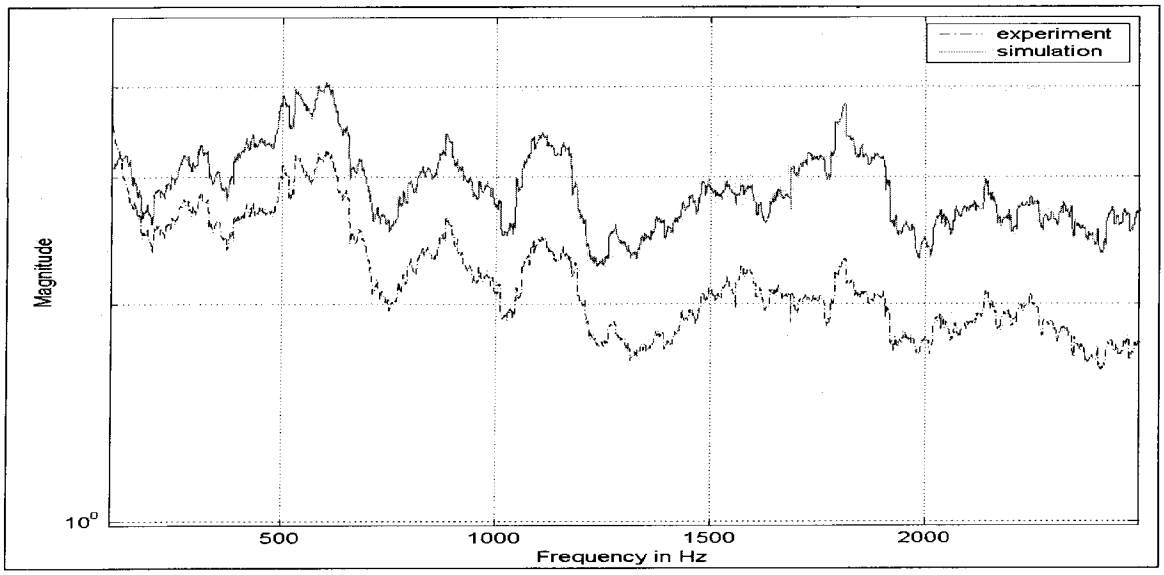

Figure A5: Frequency Response at Pt 3 in Y Direction

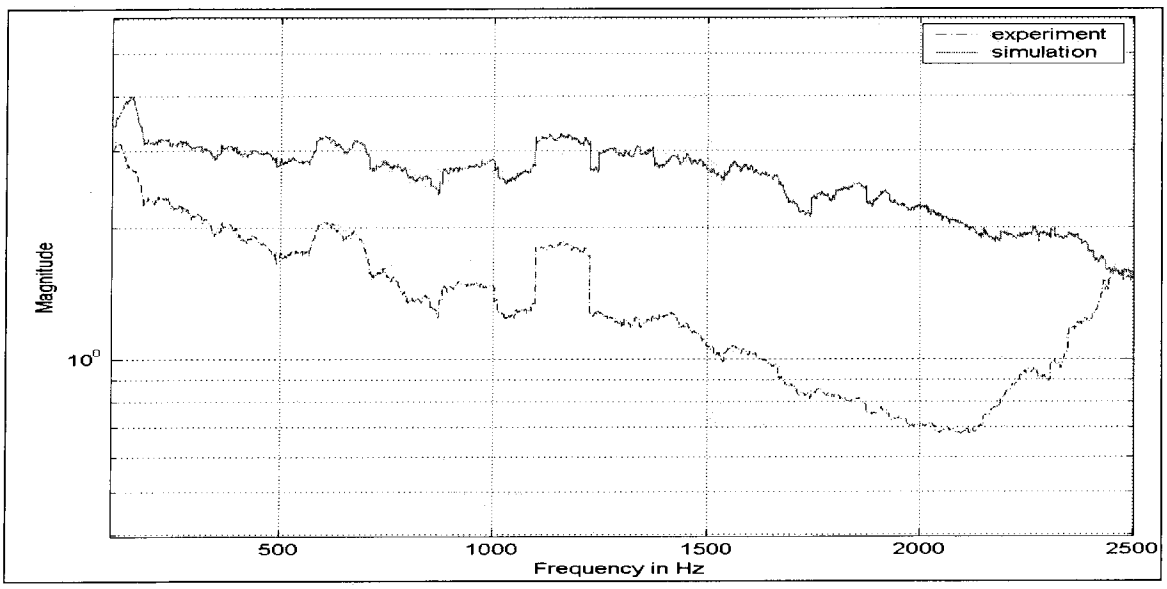

Figure A6: Frequency Response at Pt 3 in Z Direction

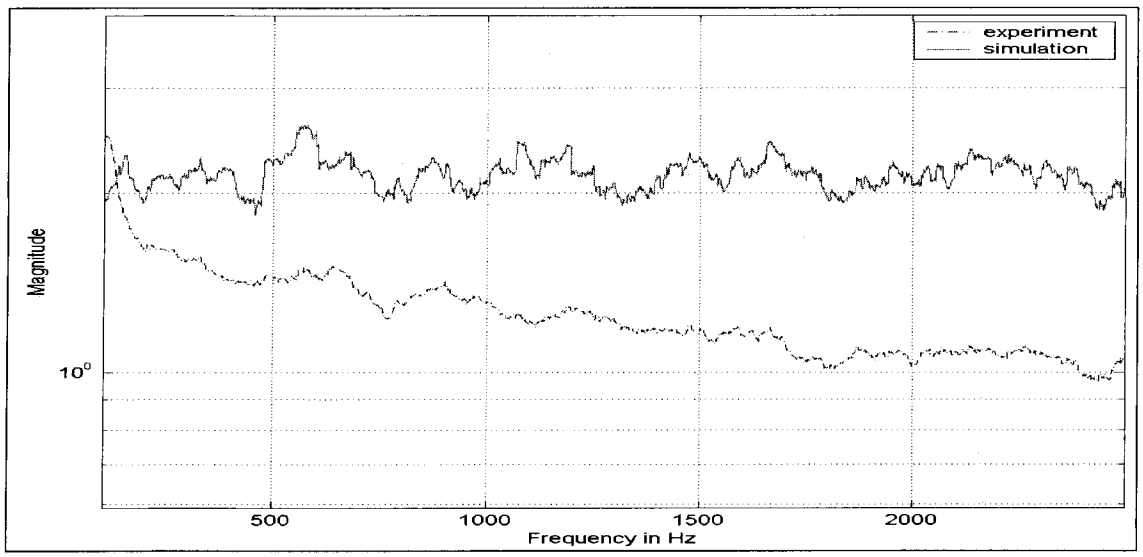

Figure A7: Frequency Response at Pt 4 in X Direction

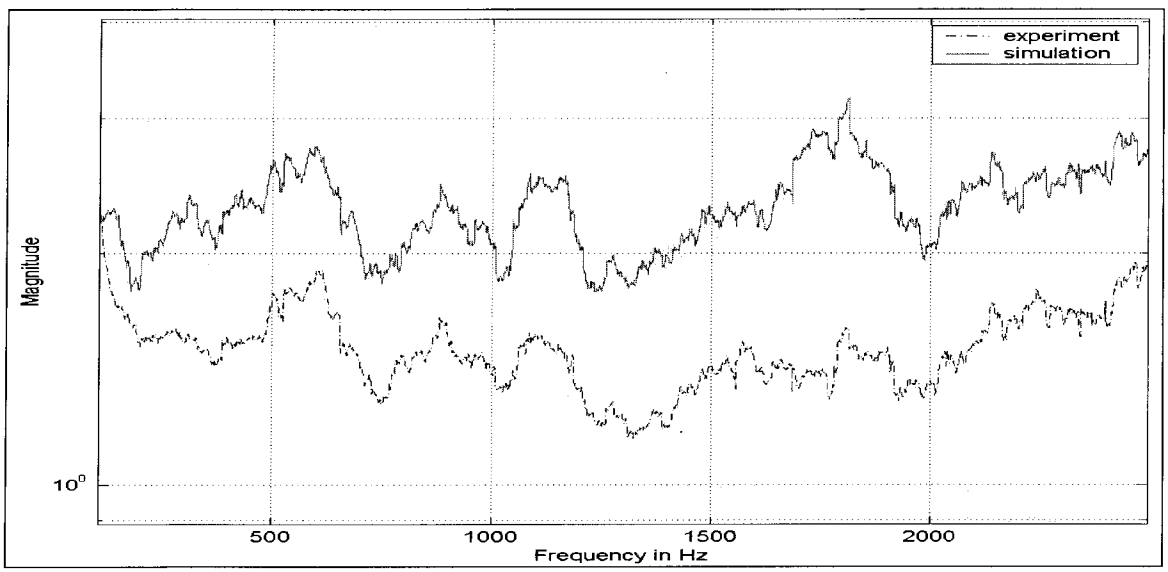

Figure A8: Frequency Response at Pt 4 in Y Direction

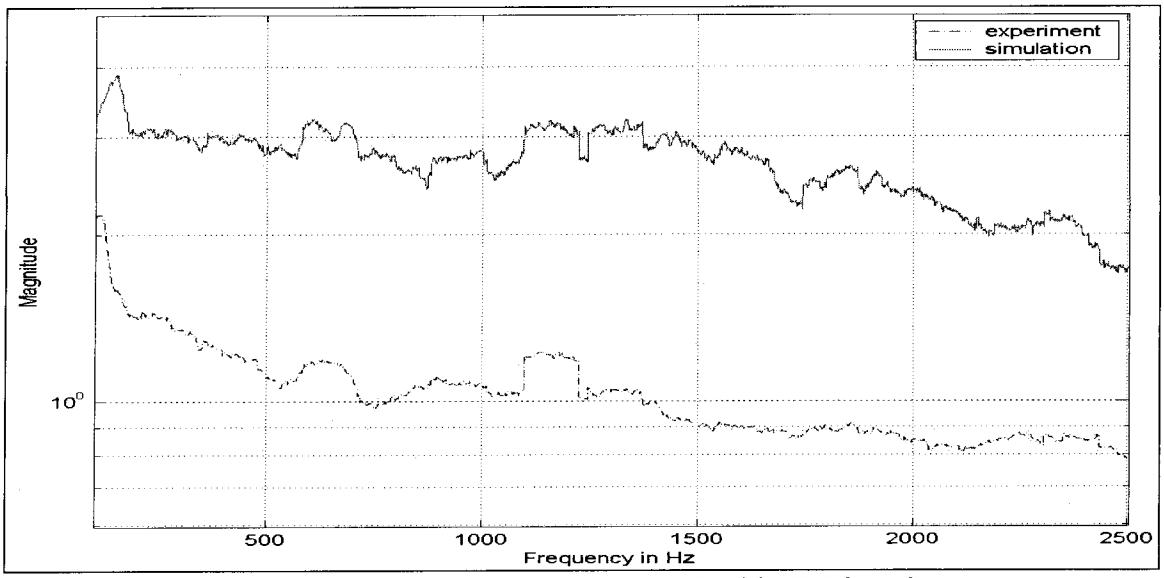

Figure A9: Frequency Response at Pt 4 in Z Direction

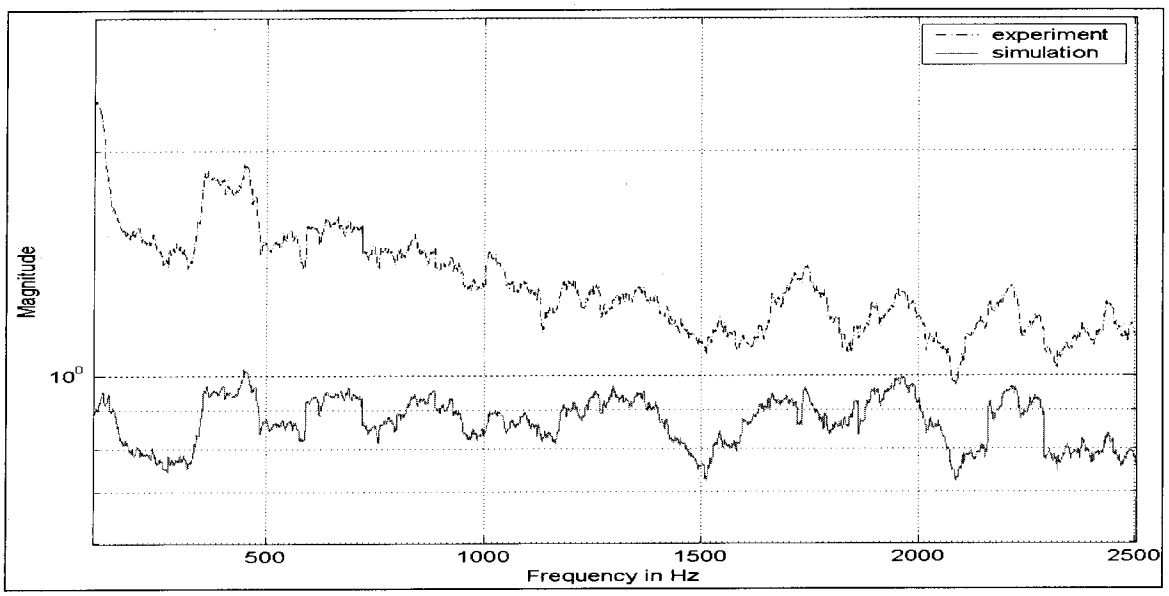

Figure A10: Frequency Response at Pt 12 in X Direction

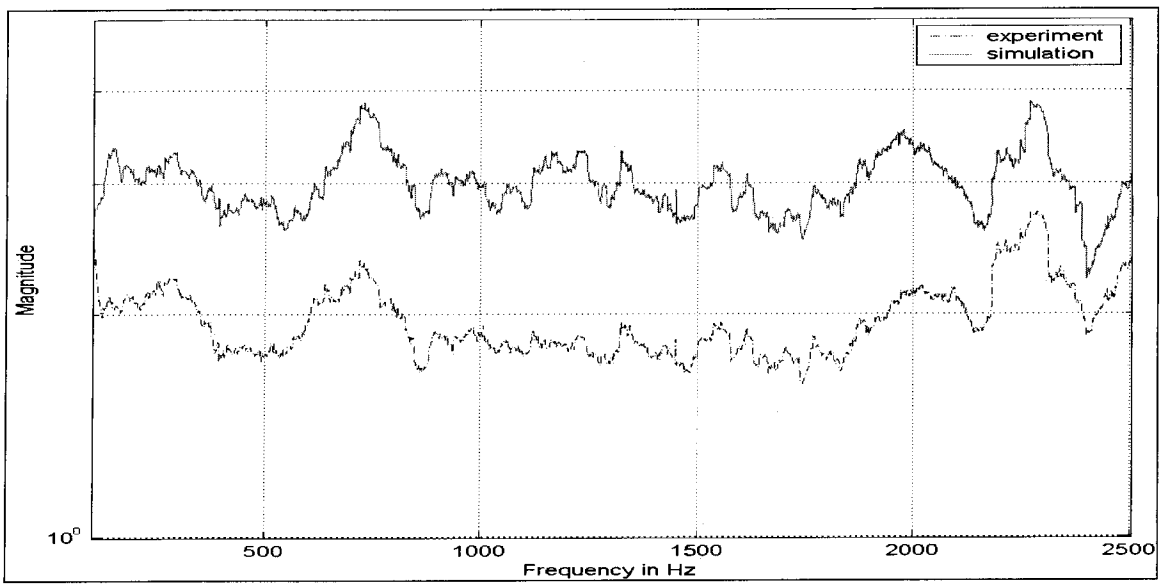

Figure A11: Frequency Response at Pt 12 in Y Direction

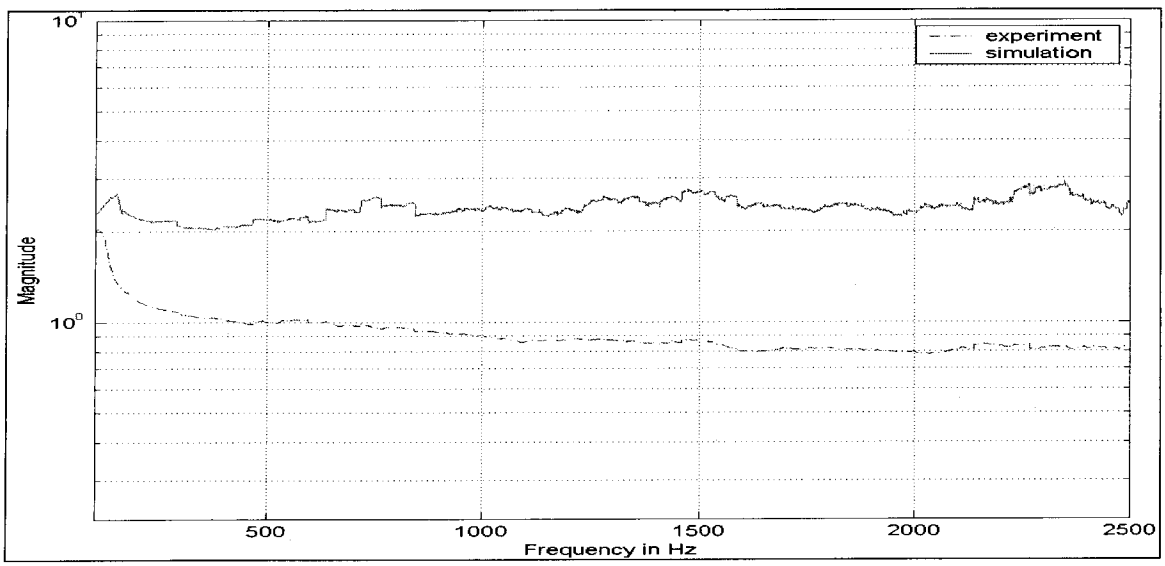

Figure A12: Frequency Response at Pt 12 in Z Direction

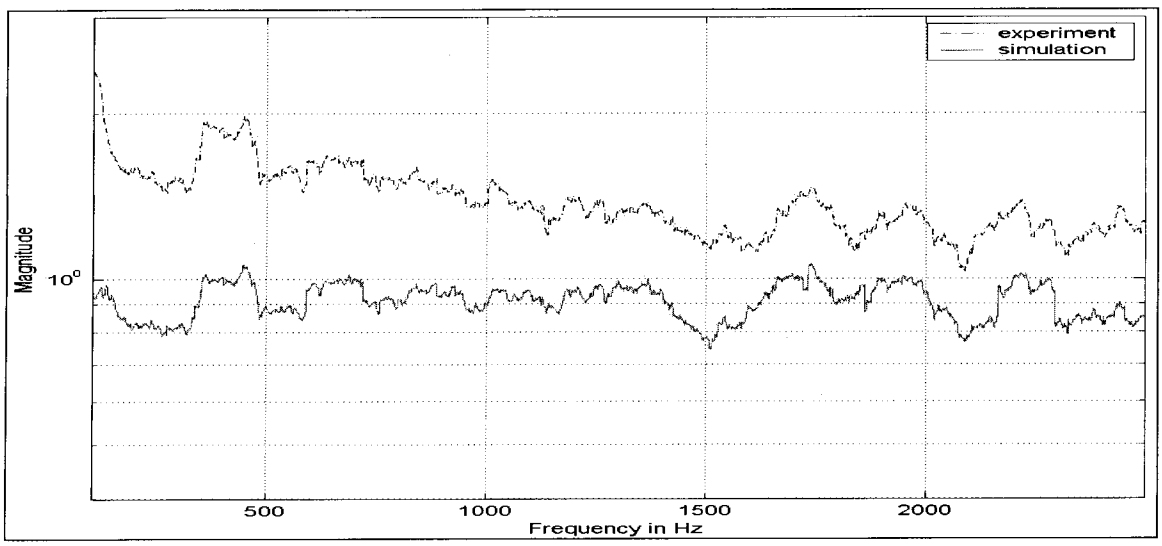

Figure A13: Frequency Response at Pt 13 in X Direction

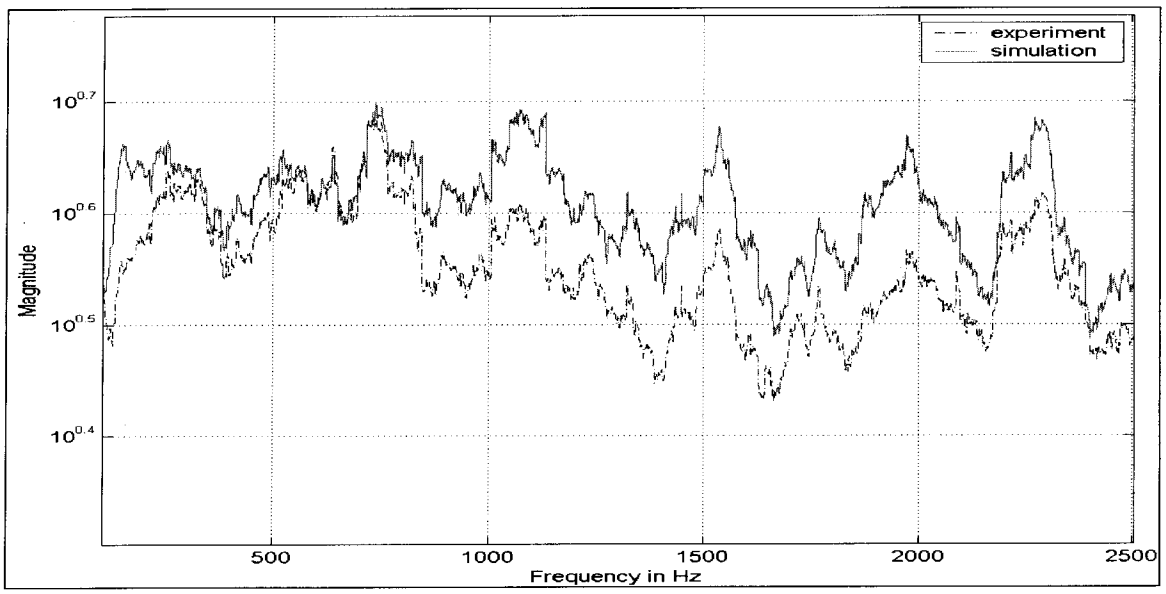

Figure A14: Frequency Response at Pt 13 in Y Direction

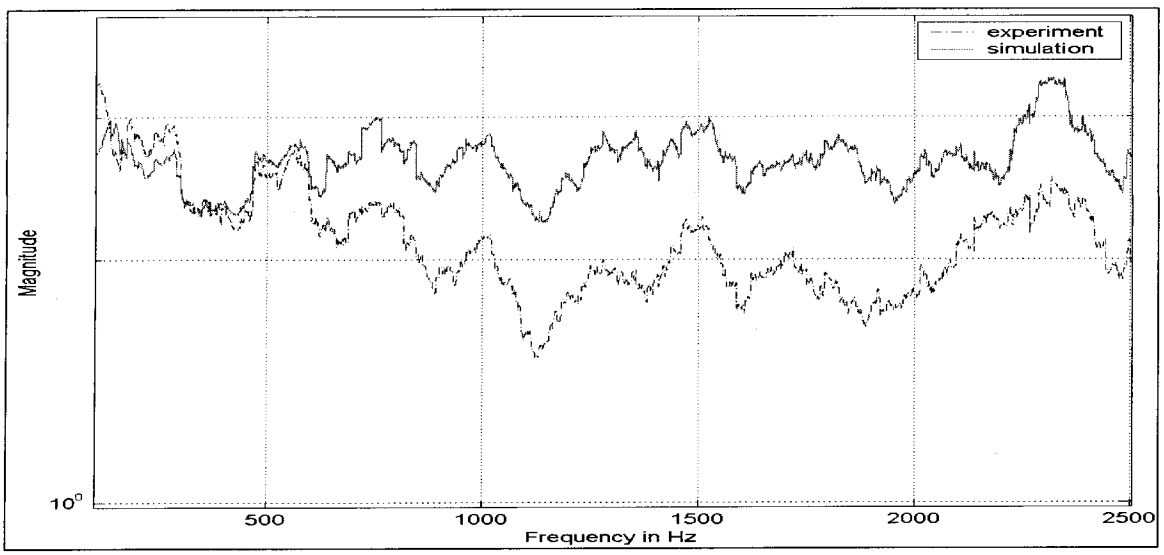

Figure A15: Frequency Response at Pt 13 in Z Direction

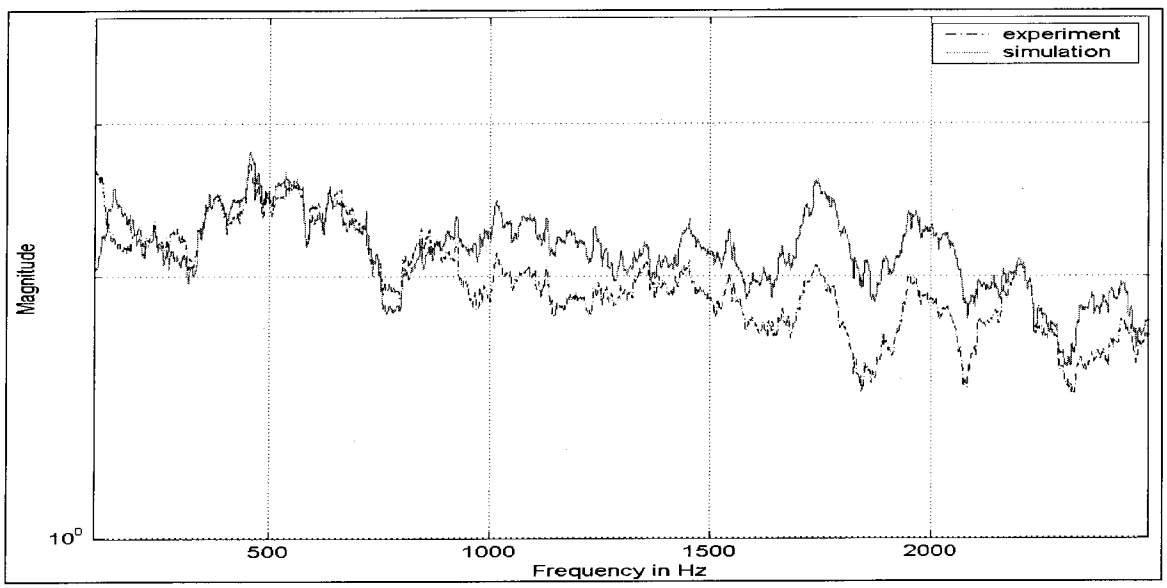

Figure A16: Frequency Response at Pt 14 in X Direction

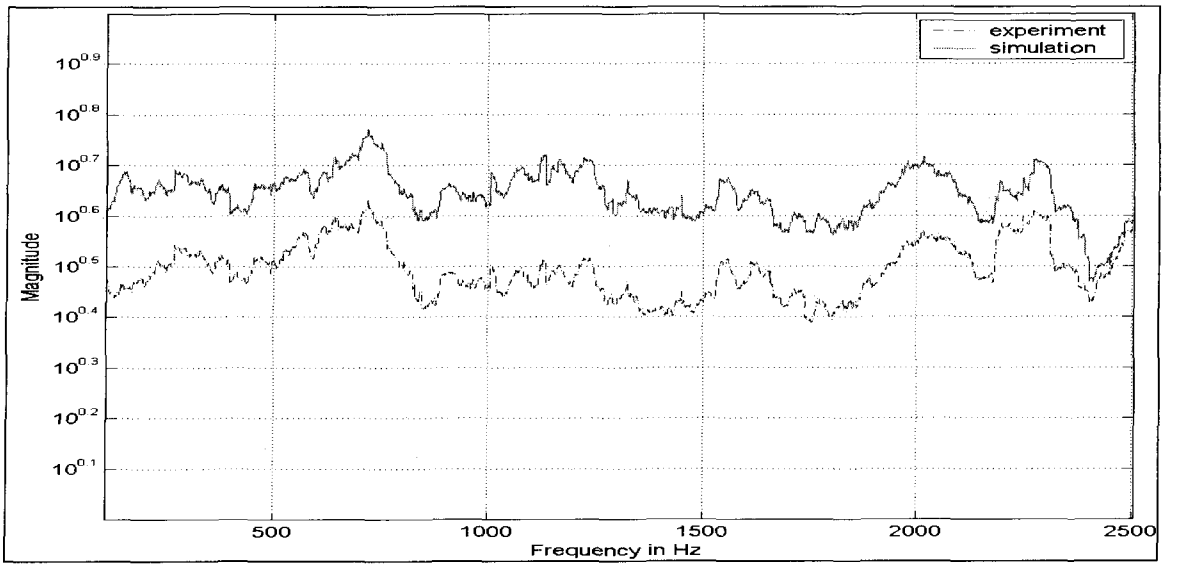

Figure A17: Frequency Response at Pt 14 in Y Direction

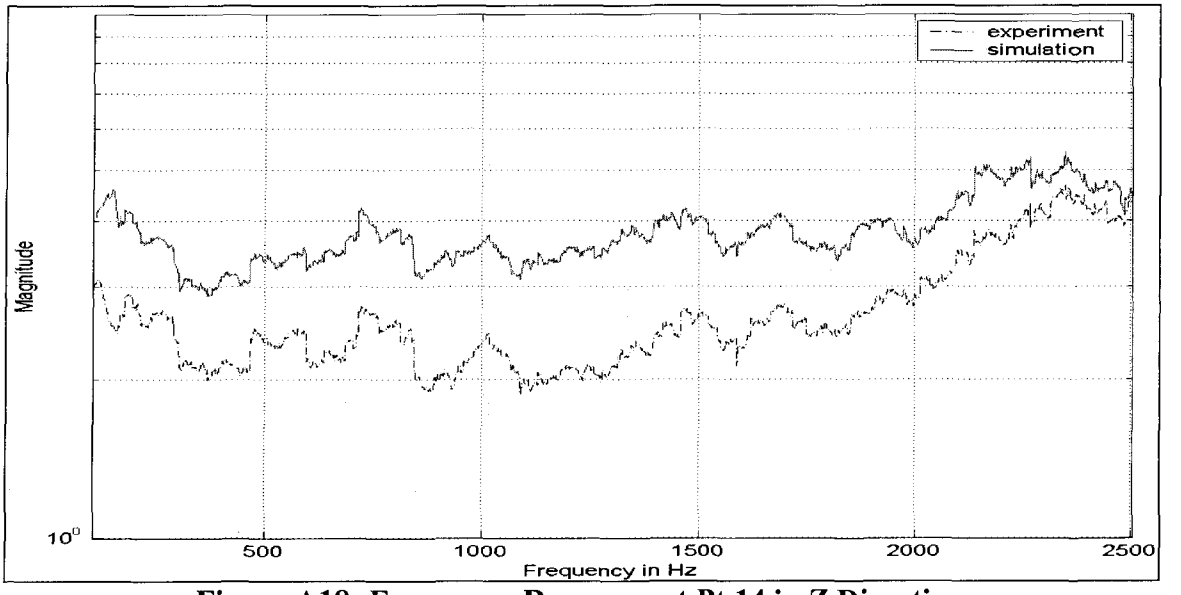

Figure A18: Frequency Response at Pt 14 in Z Direction

APPENDIX B

SIX AXIS CONTROL CROSS SPECTRA

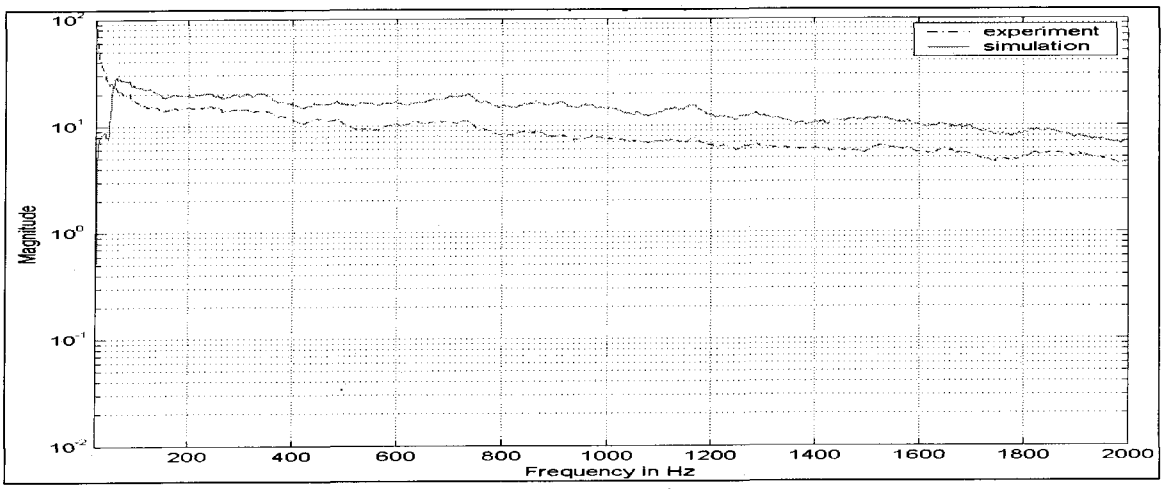

Figure B1: 8Z / X

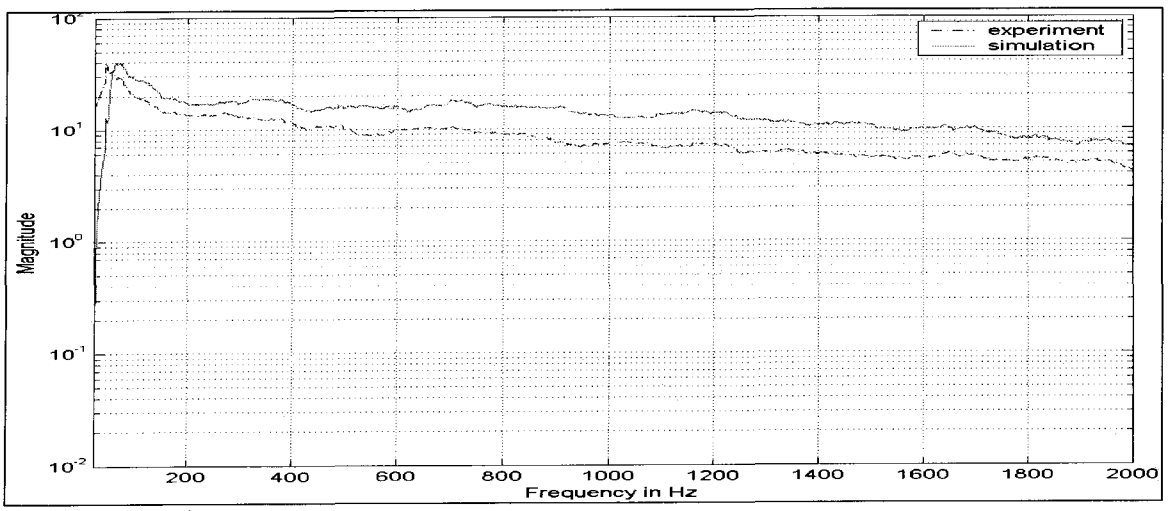

Figure B2: 8Z / Y

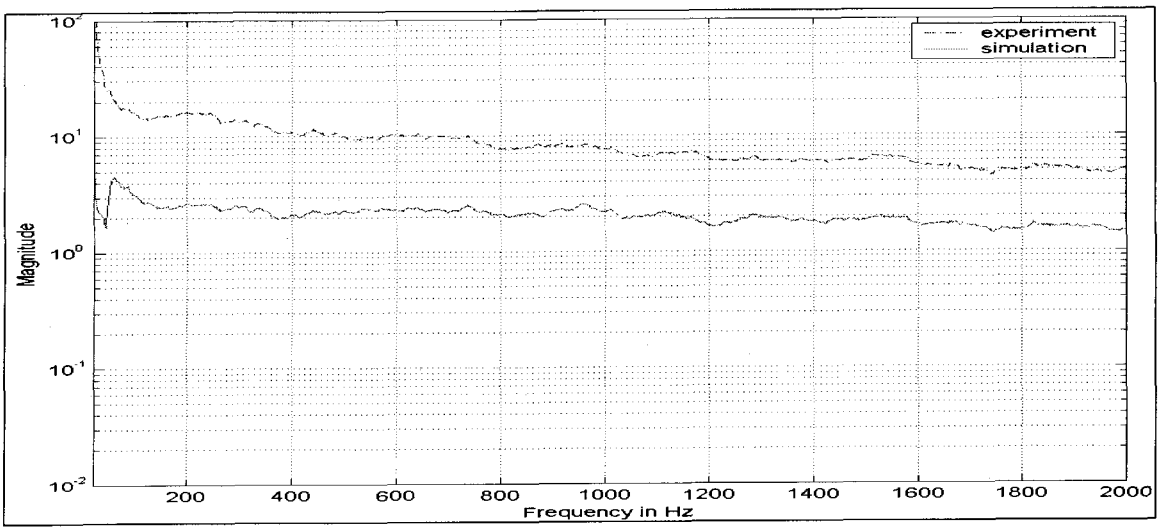

Figure B3: 13X / Y

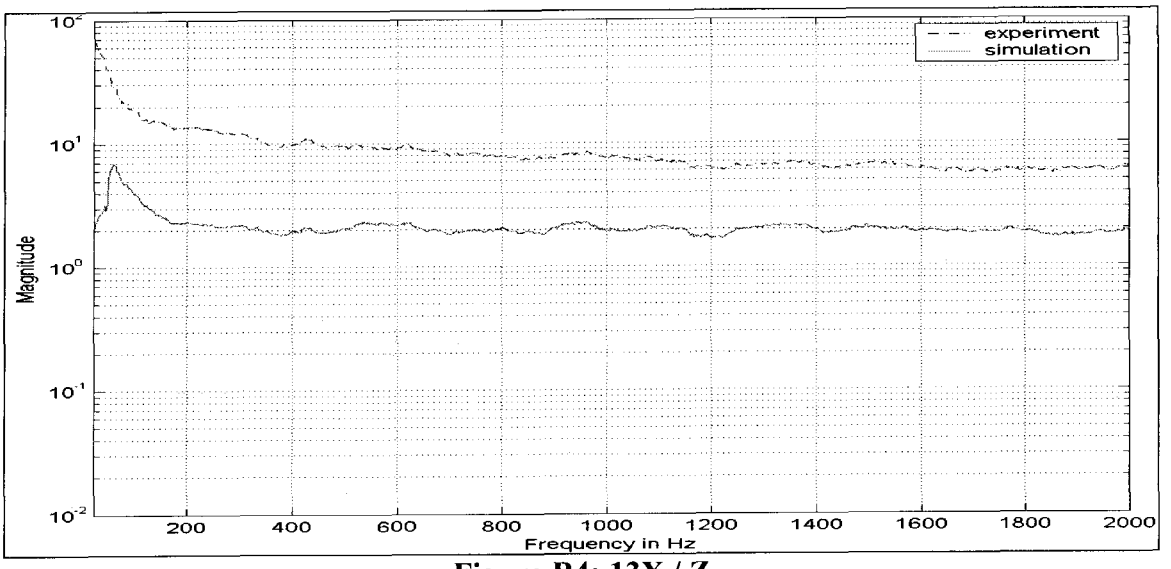

Figure B4: 13X / Z

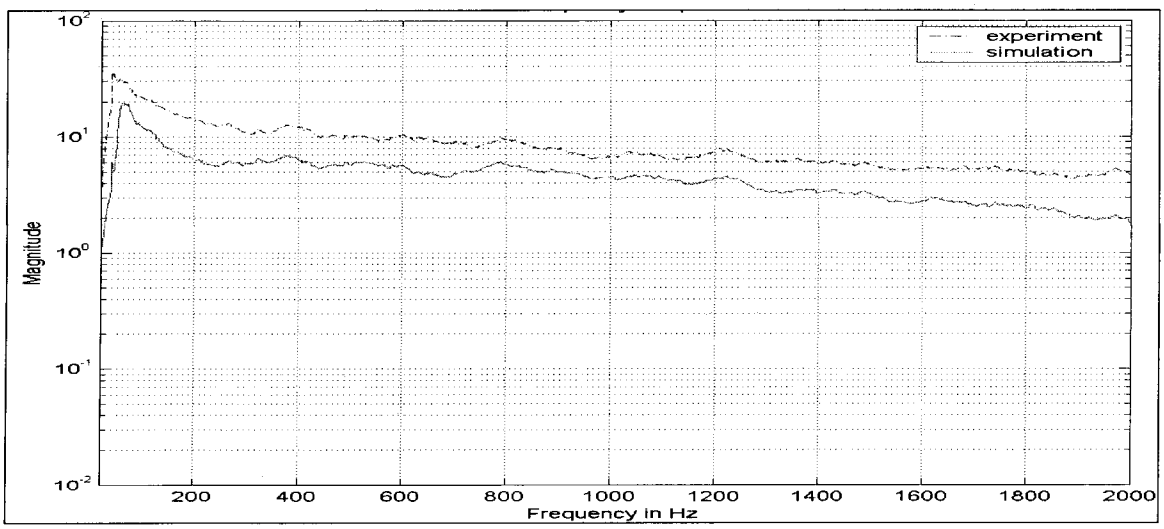

Figure B5: 13Y / X

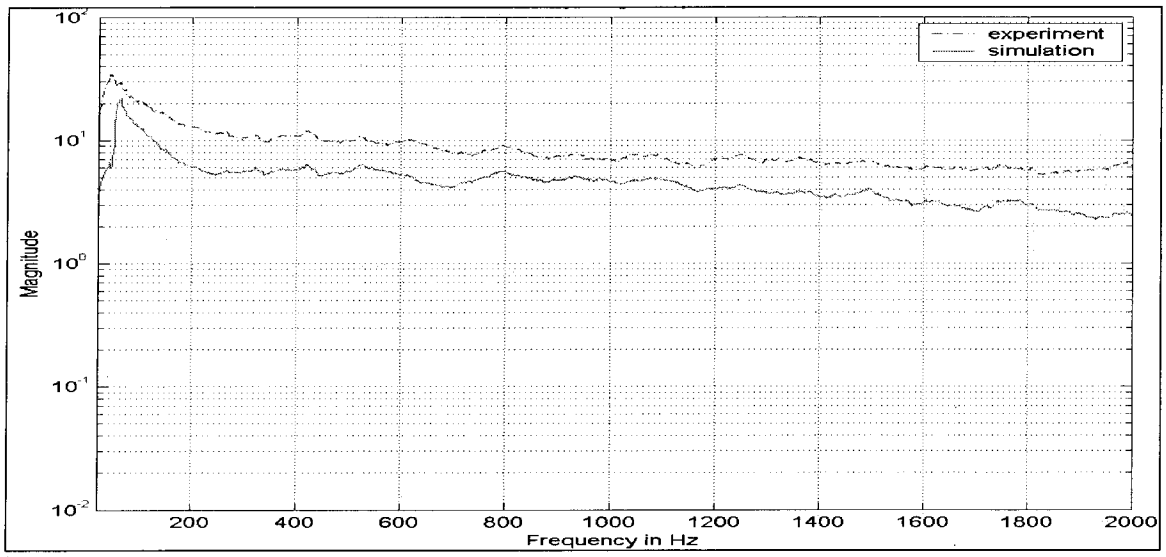

Figure B6: 13Y / Z

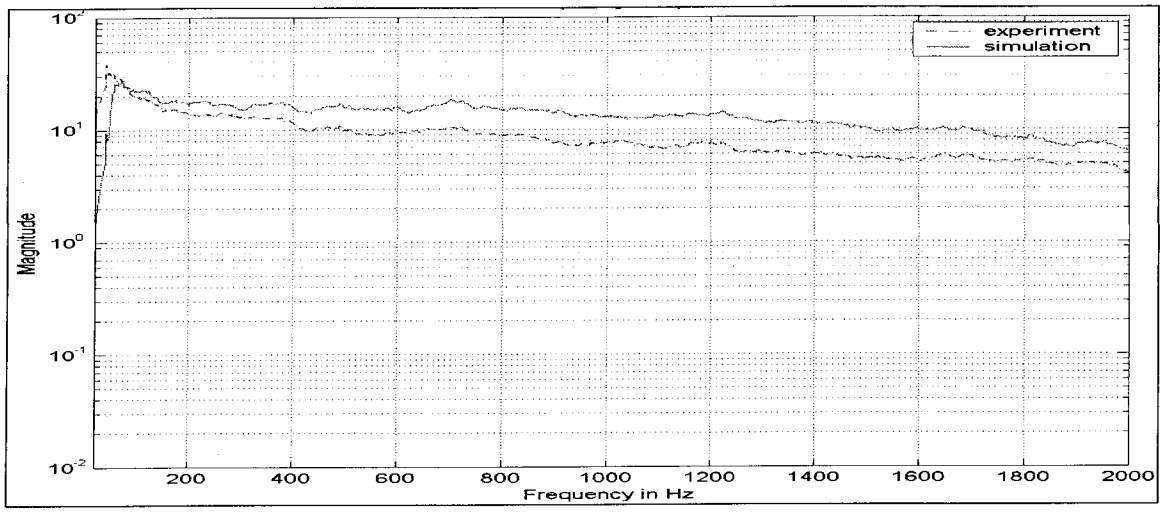

Figure B7: 13Z / X

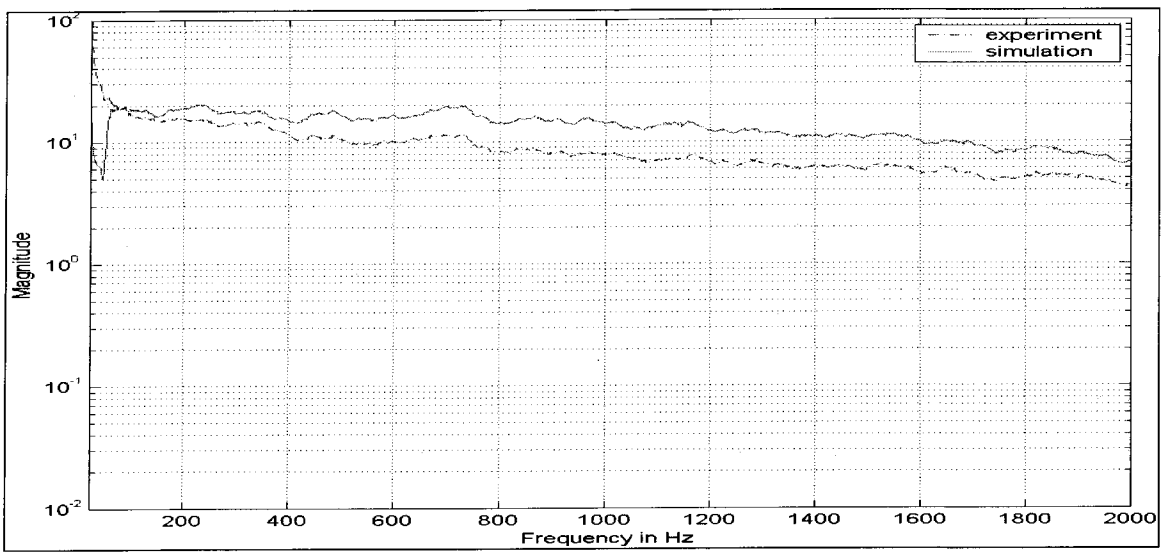

Figure B8: 13Z / Y

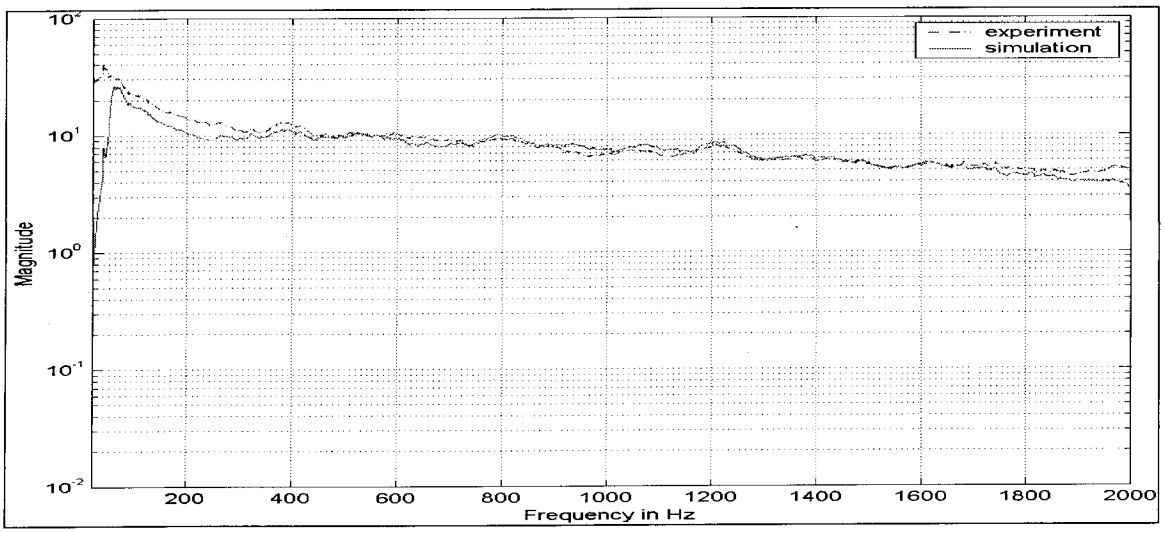

Figure B9: 14Y / X

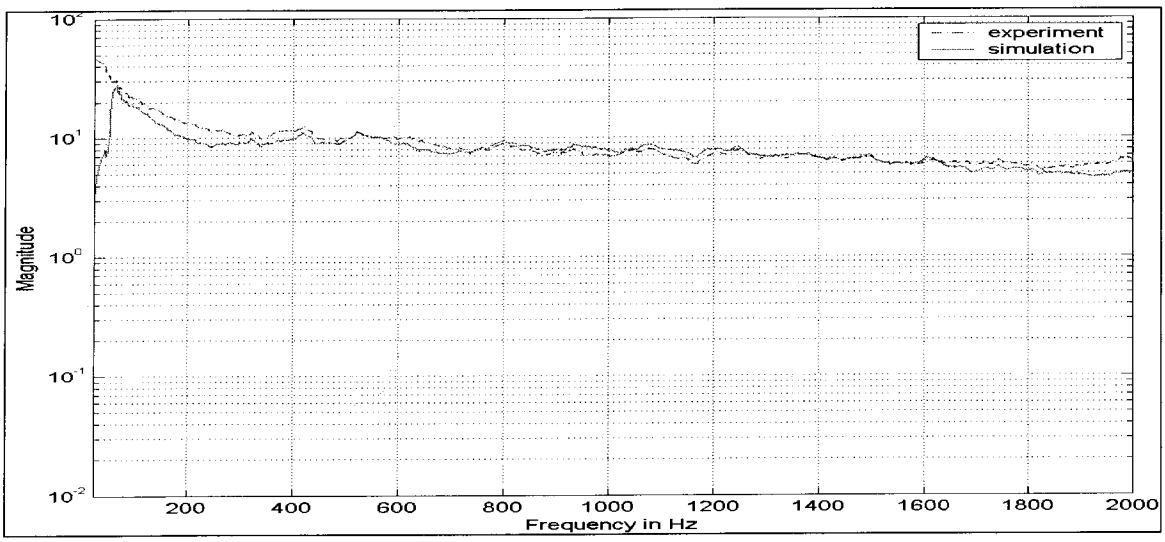

Figure B10: 14Y / Z

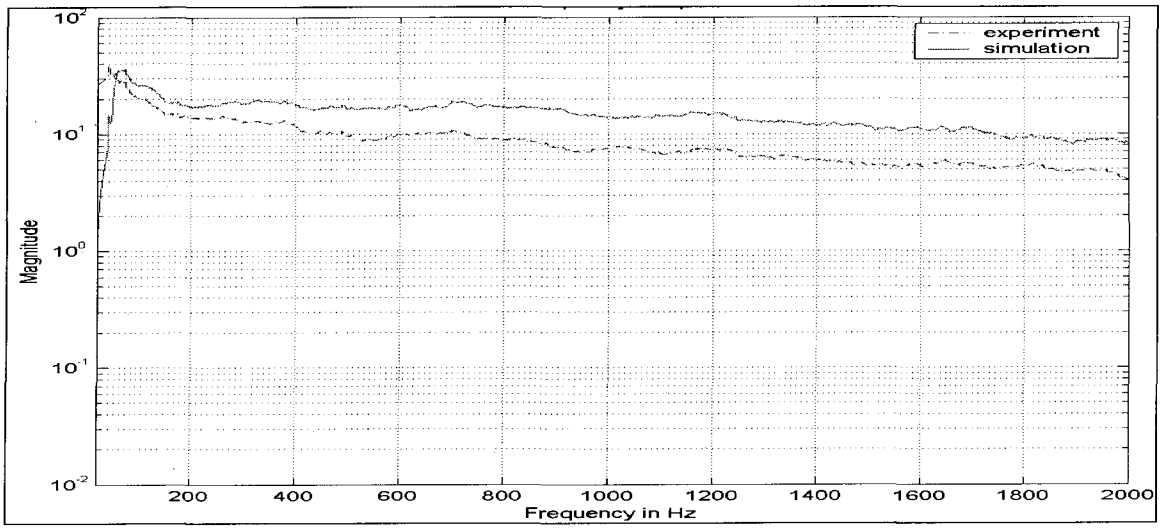

Figure B11: 14Z / X

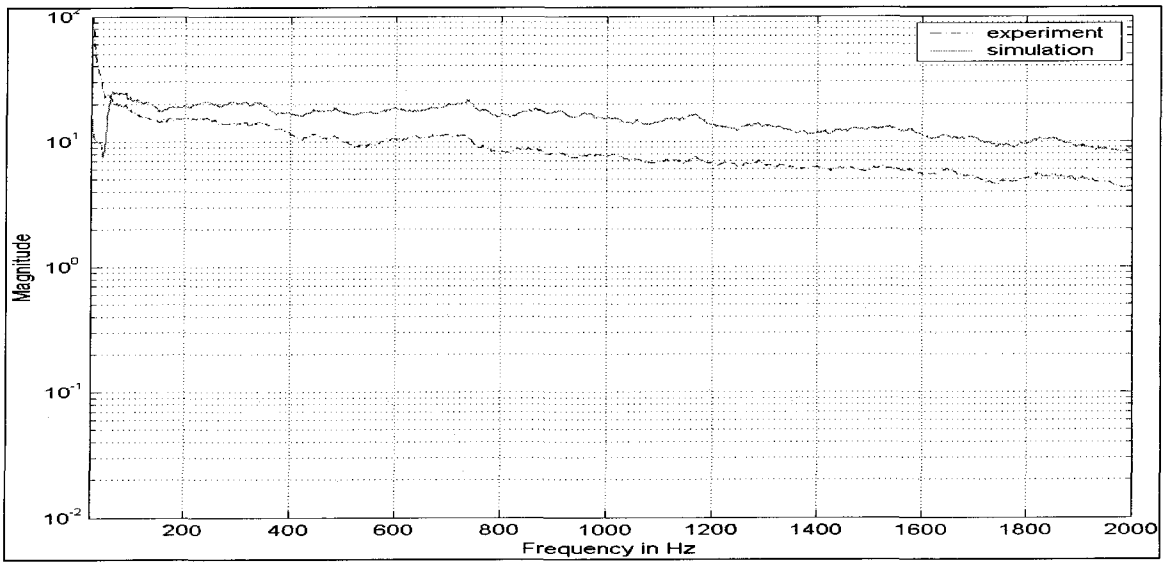

Figure B12: 14Z / Y

BIBLIOGRAPHY

[1] Nigel Cross. "Engineering Design Methods", John Wiley & Sons, London, England. 2000.

[2] Cyril Harris. "Harris' Shock and Vibration Handbook", 5th Edition, Mc Graw Hill, New York, New York. 2002

[3] George Fox, David Snyder. "Mechanical Vibrations", Dover, New York, New York. 1985.

[4] MIL Std. 810F. Department of Defense, United States of America. Test Method Standards for Environmental Engineering Considerations and Laboratory Tests. 2000.

[5] Mike Onoe. "Multi-Axis Multi-Point Vibration Tests: Excitation, Control and Analysis", IMV Corporation, Osaka, Japan. , 2002.

[6] Bruel & Kjaer. Primers, Bruel & Kjaer website http://www.bksv.com/2148.asp.

[7] Marcos A. Underwood. "Rectangular Control of Multi-Shaker Systems; Theory and practice". Institutes of Environmental Sciences and Technology Proceedings. 2002.

[8] Marcos A. Underwood, Tony Keller. "Applying Coordinate Transformations to Multi Degree of Freedom Shaker Control" Sound and Vibration Magazine. 2006

[9] TEAM TENSOR Vibration Test System Brochure

[10] Jens T. Broch, George Fox Lang. "Understanding the Physics of Electrodynamic shakers". Sound and Vibration Magazine. 2001

[11] Pedro Iniago Santiago, "Design and Optimization of a Calibration Electrodynamic Shaker", Master's Thesis, University of Puerto Rico. 2002.

[12] David O. Smallwood, "Characterization of Electrodynamic Shakers". Journal of the Institute of Environmental Sciences. 1997.

[13] Marcos A. Underwood, Tony Keller. "Recent System Developments for Multi-Actuator Vibration Control". in Sound and Vibration Magazine. 2001.

[14] Jairo Meza Periera. "Design and Comparison of LQR and PID Type Controllers in an Electrodynamic Shaker", Master's Thesis, University of Puerto Rico. 2003.

[15] Tirupathi R. Chandrupatla, Ashok D. Belegundu, "Introduction to finite element engineering", 2nd Edition. Prentice-Hall of India, 2000.

[16] Julius S. Bendat and Allan G. Piersol. "Engineering Applications of Correlation and Spectral Density", John Wiley & Sons, New York. Chichester. Brisbane. Toronto. Singapore. 1980.

[17] John G. Proakis and Dimitris G. Manolakis, "Digital Signal Processing: Principles, Algorithms, and Applications", 3rd Edition, Prentice-Hall of India, 2002.

[18] Steven W. Smith, "The Scientist and Engineer's Guide to Digital Signal Processing". California Technical Publishing. 1997.

[19] Tony Keller, Marcos A. Underwood,. "An Application of MIMO Techniques to Satellite Testing". Proceeding-Institute of Environmental Sciences and Technology. 2001.

[20] Spectral Dynamics, "An advanced Random Shaker Control Algorithm", http://spectraldynamics.com/random_adp.htm.

[21] Gene F. Franklin, J. David Powell, Michael Workman. "Digital Control of Dynamic Systems". 3rd Edition, Addison Wesley, Massachusetts. 1998.

[22] Chi-Tsong Chen, "Linear System Theory and Design", Oxford University Press, New York. 1999.

[23] Richard C. Dorf and Robert H. Bishop. "Modern Control Systems", 9th Edition, Addison Wesley, Massachusetts. 1995

VITA

Graduate College
University of Nevada, Las Vegas

Brinda Holur Venkatesh

Local Address:
4224, Cottage Circle, Apt 4
Las Vegas, NV-89119

Degrees:
Bachelor of Engineering, Electronics and Communication Engineering, 2001
University of Mysore, India

Thesis Title:
Design and Evaluation of Multi-Axis Vibration Shaker Concepts

Thesis Examination Committee:
Chairperson, Dr. Georg F. Mauer, Ph. D
Chairperson, Dr. Eugene McGaugh, Ph. D
Committee member, Dr. Sahjendra Singh, Ph. D
Committee member, Dr. Shahram Latifi, Ph. D
Graduate College Representative, Dr. Mouses Karakouzian, Ph. D